SCIENCE CHINA
Earth Sciences

Two types of hyperthermal events in the Mesozoic-Cenozoic: Environmental impacts, biotic effects, and driving mechanisms

Xiumian HU, Juan LI, Zhong HAN and Yongxiang LI

Citation: SCIENCE CHINA Earth Sciences **63**, 1041 (2020); doi: 10.1007/s11430-019-9604-4

View online: http://engine.scichina.com/doi/10.1007/s11430-019-9604-4

View Table of Contents: http://engine.scichina.com/publisher/scp/journal/SCES/63/8

Published by the Science China Press

SCIENCE CHINA
Earth Sciences

•REVIEW•

August 2020 Vol.63 No.8: 1041–1058
https://doi.org/10.1007/s11430-019-9604-4

Two types of hyperthermal events in the Mesozoic-Cenozoic: Environmental impacts, biotic effects, and driving mechanisms

Xiumian HU*, Juan LI, Zhong HAN & Yongxiang LI

State Key Laboratory of Mineral Deposit Research, School of Earth Sciences and Engineering, Nanjing University, Nanjing 210023, China

Received August 20, 2019; revised February 24, 2020; accepted March 30, 2020; published online May 19, 2020

Abstract A deeper understanding of hyperthermal events in the Earth's history can provide an important scientific basis for understanding and coping with global warming in the Anthropocene. Two types of hyperthermal events are classified based on the characteristics of the carbon isotope excursion (CIE) of the five representative hyperthermal events in the Mesozoic and Cenozoic. The first type is overall characterized by negative CIEs (NCHE) and represented by the Permian-Triassic boundary event (PTB, ~252 Ma), the early Toarcian oceanic anoxic event (TOAE, ~183 Ma), and the Paleocene-Eocene Thermal Maximum event (PETM, ~56 Ma). The second type is overall characterized by positive CIEs (PCHE) and represented by the early Aptian oceanic anoxic event (OAE1a, ~120 Ma) and the latest Cenomanian oceanic anoxic event (OAE2, ~94 Ma). Hyperthermal events of negative CIEs (NCHE), lead to dramatic changes in temperature, sedimentation, and biodiversity. These events caused frequent occurrence of terrestrial wildfires, extreme droughts, acid rain, destruction of ozone layer, metal poisoning (such as mercury), changes in terrestrial water system, and carbonate platform demise, ocean acidification, ocean anoxia in marine settings, and various degree extinction of terrestrial and marine life, especially in shallow marine. In contrast, hyperthermal events of positive CIEs (PCHE), result in rapid warming of seawater and widespread oceanic anoxia, large-scale burial of organic matter and associated black shale deposition, which exerted more significant impacts on deep-water marine life, but little impacts on shallow sea and terrestrial life. While PCHEs were triggered by volcanism associated with LIPs in deep-sea environment, the released heat and nutrient were buffered by seawater due to their eruption in the deep sea, thus exerted more significant impacts on deep-marine biota than on shallow marine and terrestrial biota. This work enriches the study of hyperthermal events in geological history, not only for the understanding of hyperthermal events themselves, large igneous provinces, marine and terrestrial environment changes, mass extinctions, but also for providing a new method to identify the types of hyperthermal events and the inference of their driving mechanism based on the characteristics of carbon isotopic excursions and geological records.

Keywords Hyperthermal events, Paleoclimate, Paleoceanography, Sedimentary record, Large igneous province, Mesozoic and Cenozoic, Deep-time

Citation: Hu X, Li J, Han Z, Li Y. 2020. Two types of hyperthermal events in the Mesozoic-Cenozoic: Environmental impacts, biotic effects, and driving mechanisms. Science China Earth Sciences, 63: 1041–1058, https://doi.org/10.1007/s11430-019-9604-4

1. Introduction

The Intergovernmental Panel on Climate Change (IPCC) Special Report "1.5°C global warming" in October 2018 shows that the Earth's annual mean temperature has risen by (1±0.2)°C since the industrial revolution (AD 1850) and continues to increase at a rate of 0.2°C per decade (IPCC, 2018). Global warming is also supported by continuous observations of the Earth's surface temperatures and seawater temperatures over the past 30 years. Greenhouse gas emissions released by human activities (mainly fossil fuel emissions) are considered to be the main cause of global

* Corresponding author (email: huxm@nju.edu.cn)

warming (Waters et al., 2016). Both society and the scientific community are concerning about whether the continuing increase in atmospheric CO_2 will cause the global climate to change from an icehouse climate, manifested by polar ice caps, to a greenhouse climate of no polar ice caps. It is imperative for the sustainability of human civilization to deepen understanding of these changes and their environmental and ecological effects.

To date, predictions of warming trends and the possible climate, ecological, and environmental changes mainly depend on climate simulations. Unfortunately, the understanding of the climatic mechanisms is neither thorough nor comprehensive. The temporal-spatial resolutions of climate models need to be further refined, and the constraints on climate parameters need to be improved. Therefore, climate simulations still have large uncertainties. Understanding the past global warming and its eco-environment effects from geological perspective will provide important insight. The Earth's climate has changed dynamically over geological history, including icehouse climates and greenhouse climates. Each climate state included a series of extreme climate events, such as extreme cooling events (Snowball Earth) and hyperthermal events, respectively. Multiple hyperthermal events occurred in the Mesozoic and Cenozoic, including the characteristic Permian-Triassic boundary event (PTB), the early Toarcian oceanic anoxic event (TOAE, Early Jurassic), the early Aptian oceanic anoxic event (OAE1a, Early Cretaceous), the Cenomanian-Turonian oceanic anoxic event (OAE2, mid-Cretaceous) and the Paleocene-Eocene Thermal Maximum (PETM) (Figure 1) (Foster et al., 2018). This study provides a comprehensive review of these hyperthermal events. By summarizing the onset duration, the extent and rate of warming, environmental and ecological changes of these events, we divide these events into two types based on their characteristic carbon isotope excursions. In addition, by systematically comparing the environmental and ecological effects between these two types of hyperthermal events, we propose that the different responses of these two types of hyperthermal events were closely related to the different eruption environments where large igneous provinces (LIPs) were formed. This study could provide scientific references for better understanding and coping with the current global warming.

2. Carbon isotopic characteristics and classification of the five hyperthermal events in the Mesozoic and Cenozoic

2.1 Carbon isotopic characteristics of the five hyperthermal events

The PTB event occurred at the end of the Permian (~252 Ma) and shows the largest warming magnitude (~8–10°C) in the Phanerozoic (Joachimski et al., 2012; Sun et al., 2012; Shen et al., 2019) (Table 1). It has also been shown to be lower than 6°C (Brand et al., 2012; Cui and Kump, 2015). The bulk carbon isotopes experienced at least three cycles of negative-excursion-then-recovery during the PTB event with a large negative excursion of more than −7‰ (Cao et al., 2009).

The TOAE occurred in the Early Jurassic (~183 Ma) with a warming magnitude of 7–10°C in the middle latitudes in the northern hemisphere (Suan et al., 2008a; Dera et al., 2009; Korte et al., 2015) (Table 1). The negative CIE of TOAE is characterized by a magnitude of −3‰ to −8‰ and consists of several secondary negative excursions (Kemp et al., 2005; Jenkyns, 2010).

The OAE1a is also called the Livello Selli event and occurred at early Aptian in the early Cretaceous (~120 Ma) with a warming of 5–6°C at low latitudes and 2–4°C at mid-to-high latitudes (Mutterlose et al., 2010, 2014; Naafs and Pancost, 2016). The CIE is characterized by an extremely negative excursion and then a 2–5‰ positive excursion (Menegatti et al., 1998).

The OAE2 is also known as the Bonarelli Event and occurred at the end of the Cenomanian (~94 Ma). The warming of 2–3°C in low latitudes, 4–5°C in middle latitudes, and 7–10°C in high latitudes are reported (Jenkyns et al., 2004; Forster et al., 2007; Huber et al., 2018) (Table 1). The CIE was overall positive with a magnitude generally greater than 2‰ (Jenkyns, 2010), but appears to show a weak negative excursion before the positive excursion in an expanded section (Li Y X et al., 2017).

The PETM was a hyperthermal event that occurred at the Paleocene-Eocene boundary (~55.8 Ma) (Kennett and Stott, 1991; Zachos et al., 2001). This event shows, on average, ~4–5°C warming of global sea surface temperature (Dunkley Jones et al., 2013), 3°C at low latitudes (Frieling et al., 2017), and 5–8°C at mid-to-high latitudes (Sluijs et al., 2006, 2011; Zachos et al., 2006) (Table 1). The CIE shows a rapid negative shift, and then a 2–7‰ negative shift prior to the final recovery (Kennett and Stott, 1991; McInerney and Wing, 2011).

2.2 Classification and stage divisions of the five hyperthermal events based on the CIE features

Based on the CIE characteristics, we divided these five hyperthermal events into two types: Negative CIE Hyperthermal Event (NCHE) and Positive CIE Hyperthermal Event (PCHE).

The NCHE events show negative CIEs, and include the PTB, TOAE and PETM (Figure 2). These events show a broad negative CIE from background carbon isotope values, and the pre- and post-event stage is denoted as NC1 and NC5, respectively. The broad negative CIE consists of an initial one-step (PETM, TOAE) or stepwise (PTB) negative

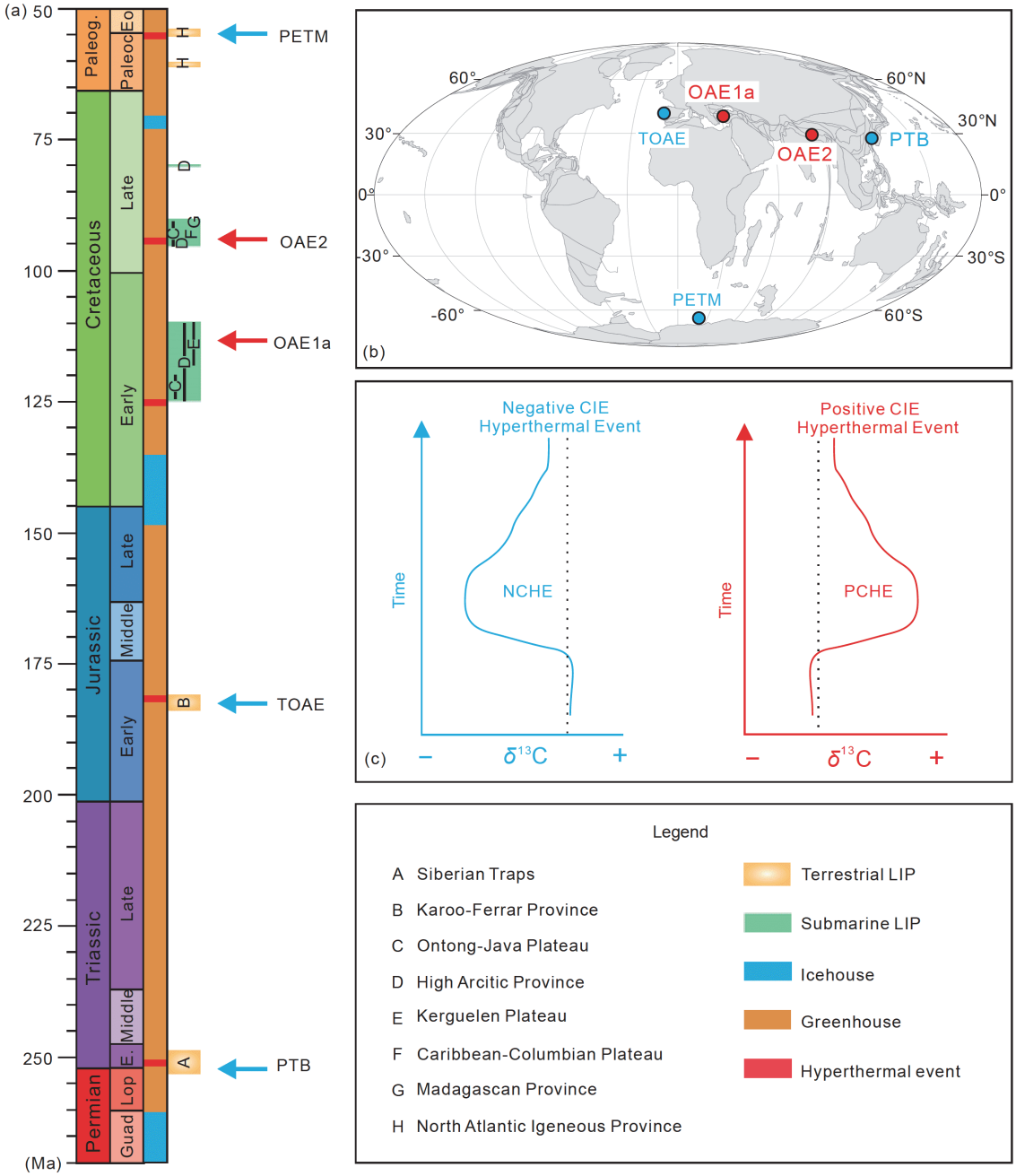

Figure 1 (a) An illustration of the middle Permian to Eocene timescale (Ogg et al., 2016), showing ages of the five Mesozoic and Cenozoic environmental perturbations, LIP emplacements, and the Earth's climate (NRC 2011). (b) Geographical map showing the locations mentioned in our studies (www.odsn.de). PTB: Meishan section, Zhejiang; Burgess et al., 2014. TOAE: Peniche section, Portugal; Hesselbo et al., 2007. OAE1a: Yenicesilar section, Turkey; Hu et al., 2012. OAE2: Gongzha section, southern Tibet; Li Y X et al., 2017. PETM: ODP site 690, Southern Ocean; Bains et al., 1999. (c) The two types of hyperthermal events classified based on carbon isotopic profile: NCHE, the Negative Carbon isotopic excursion Hyperthermal Event that is characterized by a negative carbon isotopic excursion profile, and PCHE, the Positive Carbon isotopic excursion Hyperthermal Event that is characterized by a positive carbon isotopic excursion profile.

shift stage (onset stage, NC2), a stage of sustained low δ^{13}C values (the main stage, NC3), and a stage of gradual positive shift in δ^{13}C values (recovery, NC4) (Figure 2). The broad negative CIE of the NCHE events including NC2–NC4 stages, is generally thought to be caused by the injection of large amounts of light carbon into the atmosphere-ocean system.

The PCHE events are overall characterized by a broad positive CIE and are represented by OAE1a and OAE2 (Figure 3). The broad positive CIE of this type of events is preceded by a transient strong (OAE1a) or weak (OAE2) negative δ^{13}C shift. The carbon isotope variations of these events can be generally divided into four stages, an onset stage (PC2) of the transient negative δ^{13}C shift, a stage of

Table 1 Comparison of the two types hyperthermal events showing the magnitude of warming from low to high latitudes, carbon isotope excursion, and onset duration

Hyperthermal events		Duration of onnset (NC2 or PC2) (kyr)	CIE magnitude of oneset (NC2 or PC2) (‰)	Temperature (°C)			References
				Low latitude	Middle latitude	High latitude	
PCHE	OAE2	50	>2	2–3	4–5	7–10	Jenkyns et al. (2004), Forster et al. (2007), Huber et al. (2018)
	OAE1a	75	2–5	5–6	2–4	2–3	Mutterlose et al. (2010), Naafs and Pancost (2016)
NCHE	PETM	3	−2–−6	3–5	6–8	5–9	Thomas et al. (2002), Zachos et al. (2003, 2006), Aze et al. (2014), Sluijs et al. (2011, 2014)
	TOAE	150	−3–−8	–	7–10	–	Suan et al. (2008a), Dera et al. (2009), Korte et al. (2015)
	PTB	60	>−7	8–10	–	–	Sun et al. (2012), Joachimski et al. (2012), Burgess et al. (2014), Chen et al. (2016)

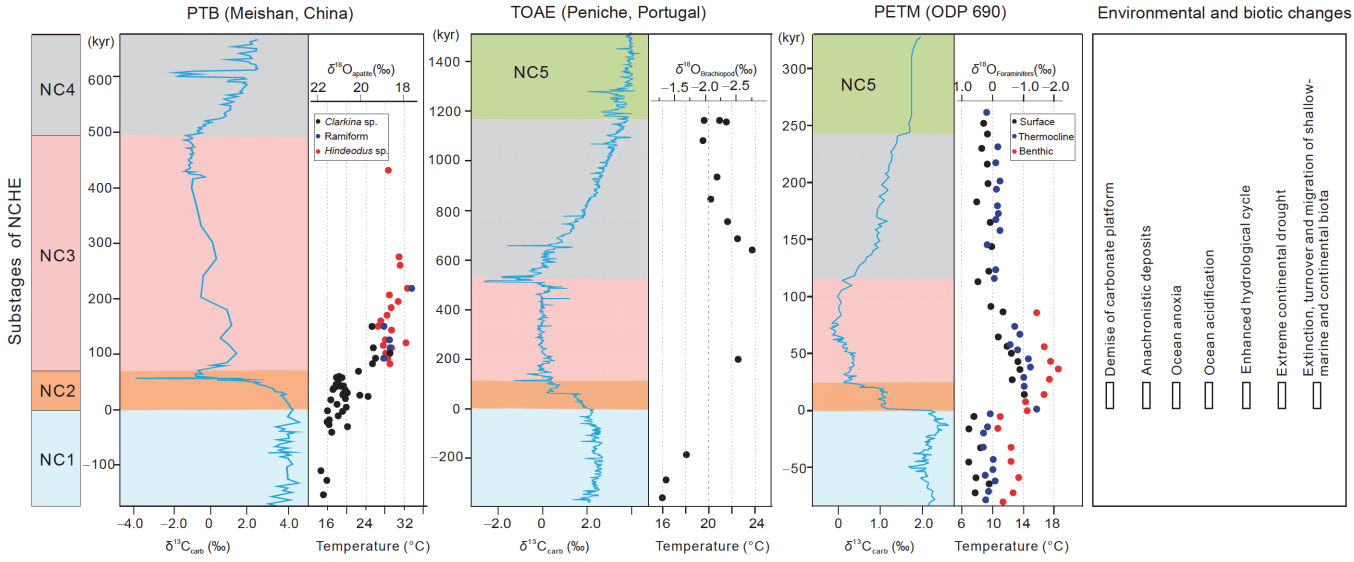

Figure 2 Characteristics of carbon isotopic profile and temperature across the NCHE including PTB, TOAE and PETM, and their environmental and biotic effects. The negative CIE of the NCHEs can be broadly divided into four stages: an onset stage NC2, represented by one (PETM, TOAE) or multiple (PTB) negative excursion (NC2, onset stage), a main stage NC3, represented by an isotopic negative plateau, and a recovery stage NC4, represented by a positive excursion. The pre-NCHE interval is defined as stage NC1, and the post-NCHE interval is defined as stage NC5. Carbon isotopic and temperature data are from: PTB (Burgess et al., 2014), TOAE (Hesselbo et al., 2007; Suan et al., 2010), PETM (Bains et al., 1999; Thomas et al., 2002).

positive $\delta^{13}C$ shift (PC3), a sustained stage of enriched $\delta^{13}C$ values (main stage, PC4), and a stage of gradual decrease of $\delta^{13}C$ values (recovery stage, PC5) (Figure 3). These events were generally thought to be caused by transient injection of massive light carbon into the atmosphere-ocean system, which triggered anoxia in bottom water and large-scale burial of organic-rich black shales, leading to a broad positive CIE.

3. Timescale and duration of the two types of hyperthermal events in the Mesozoic and Cenozoic

With the high-precision dating and the application of cyclostratigraphy in recent years, durations of these two types of hyperthermal events have been much better constrained, allowing for discussing warming rates of each type of hyperthermal events. It is worth noting that duration estimates of each event are usually obtained from cyclostratigraphy that is anchored by the high-precision U-Pb age of zircon in tuff layer. Interpolation with an average sedimentation rate within an orbital cycle is often used to obtain the CIE durations of these events. This analytical technique generally carries uncertainties of about 10–100 kyr.

3.1 Timescale and duration of the NCHE

The timescale of the PTB event is mainly based on high-precision U-Pb chronology of zircon from the global stratotype section and point (GSSP) section of the Permian-Triassic boundary in South China (Shen et al., 2011, 2019; Burgess et al., 2014), combined with carbon isotope stratigraphy (Cao et al., 2009). The PTB duration was constrained

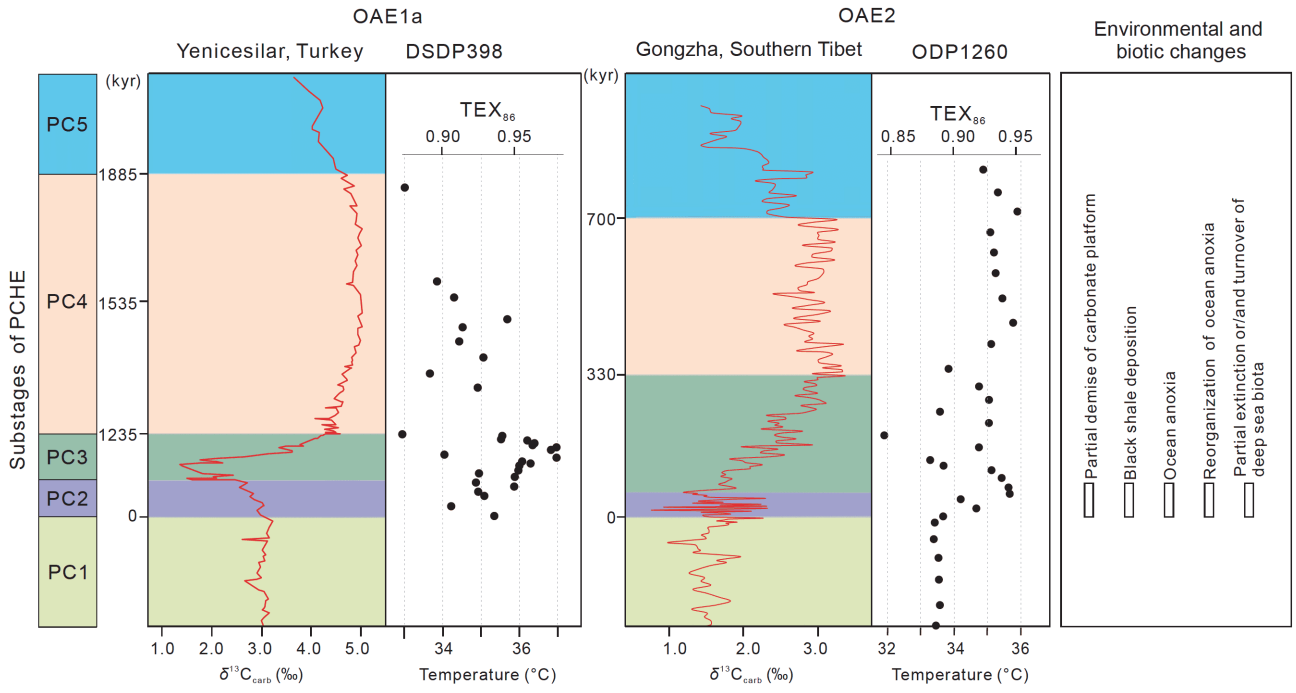

Figure 3 Characteristics of carbon isotopic profile and temperature across the PCHEs including OAE1a and OAE2, and their environmental and biotic effects. The positive carbon isotopic excursion of the PCHEs can be subdivided into four stages: an onset stage PC2, a positive excursion stage PC3, a main stage PC4 as represented by an isotopic positive plateau, and a recovery stage PC5. The pre-PCHE interval is defined as stage PC1, and the post-PCHE interval is defined as stage PC6. Carbon isotopic and temperature data are from: OAE1a (Hu et al., 2012; Naafs and Pancost, 2016), OAE2 (Forster et al., 2007; Li Y X et al., 2017).

to ~660 kyr (Burgess et al., 2014), of which the onset (NC2) duration is ~58 kyr, the duration of the sustained CIE (NC3) is ~431 kyr, and the duration of the recovery stage (NC4) is ~170 kyr (Figure 2).

There are two different duration estimate for the TOAE. One suggests that it lasted for ~900 kyr, which is based on the age constraints by cyclostratigraphy from Peniche (GSSP section) in Portugal (Suan et al., 2008b; Huang and Hesselbo, 2014). This result is consistent with that from Dotternhausen (Germany), Valdorbia (Italy), Yorkshire (UK), and Lorraine Sub-Basin (France) by cyclostratigraphy (Huang and Hesselbo, 2014; Ruebsam et al., 2014), and Yorkshire (UK) by strontium stratigraphy (McArthur et al., 2000). The duration estimate is ~300–500 kyr (Kemp et al., 2005, 2011; Boulila et al., 2014), which is mainly based on the magnetic susceptibility cyclostratigraphy from Sancerre-Couy borehole (France) and Yorkshire (UK). We employ the ~900 kyr duration of the Peniche GSSP section, and the corresponding NC2, NC3 and NC4 have a duration of ~150, ~450 and 300 kyr, respectively (Suan et al., 2008b) (Figure 2).

High-resolution timescales for the PETM have been developed using cyclostratigraphy and ^{3}He chronology, but are still controversial. The PETM duration has been constrained to 150–220 kyr by cyclostratigraphy (Röhl et al., 2003, 2007) (Figure 2), to 120–220 kyr by ^{3}He chronology (Farley and Eltgroth, 2003; Murphy et al., 2010). Recently, Westerhold et al. (2018) constructed the timescales of Ocean Drilling Program (ODP) core and continental core in Bighorn basin and constrained the duration of PETM to ~200 kyr. The PETM onset was generally considered to last at least several thousand years, ranging from 8 to 23 kyr (Zachos et al., 2005; Aziz et al., 2008; Charles et al., 2011). However, Wright and Schaller (2013) showed that the PETM onset lasted for 13 kyr based on the Millville borehole results, although this constraint was considered to result from drilling disturbances rather than the original sedimentary rhythm (Zeebe et al., 2014; Pearson and Nicholas, 2014). Regarding the duration of other CIE stages, the NC3 and NC4 stages have been estimated to be 59 and 113 kyr, respectively, based on the cyclostratigraphic data of ODP1266 borehole (Röhl et al., 2007). In contrast, these two stages were constrained to be 115 kyr (NC3) and 42 kyr (NC4), respectively, based on the cyclostratigraphic results of the Bighorn terrestrial basin (Aziz et al., 2008). Additionally, the duration of the NC3 has been calculated to be 113 kyr, and the NC4 stage can be further divided into two substages, including a rapid recovery substage (33 kyr) and a subsequent slow recovery substage (50 kyr) (Murphy et al., 2010).

3.2 Timescale and duration of the PCHE

The duration of OAE1a is mainly constrained by cyclostratigraphy. Based on the CIE characteristics, it was divided into C2–C8 stages (Menegatti et al., 1998), among which the

C3–C6 stages are constrained to be 1.0–1.3 Myr (Li et al., 2008; Bottini et al., 2012). Stage C2 shows a gradual negative $\delta^{13}C$ shift (Socorro et al., 2017), and stage C3 is characterized by sustained low $\delta^{13}C$ values. In this study, both stages C2 and C3 are combined to be defined as the transient negative $\delta^{13}C$ shift, i.e., the onset stage PC2, stages C4–C6 as the gradually positive $\delta^{13}C$ shift interval of PC3, C7 as the enriched plateau interval of PC4, and C8 as recovery stage PC5 (Figure 3). If the 1.11 Myr duration of the C3–C6 stages is applied to the Gorgo a Cerbara section, Italy, the PC2, PC3 and PC4 has a duration of 70 kyr, 1.04 Myr, and 0.75 Myr, respectively (Stein et al., 2012; Patruno et al., 2015; Li et al., 2016). In the Yenicesilar section, Turkey, the durations of the C2 and C3 stages are 75 and 320 kyr, respectively, and thus the PC2 lasted for 395 kyr (Figure 3); the durations of the PC3 and PC4–PC5 are 790 kyr and 1.3 Myr, respectively (Hu et al., 2012).

The duration of the OAE2 is also mainly constrained by cyclostratigraphy. Its duration is highly controversial, ranging from 200 to > 900 kyr (Sageman et al., 2006; Li Y X et al., 2017). In the GSSP section of Western Interior Seaway (WIS) in North America, the duration of the PC3–PC4 was constrained to be ~580 kyr, among which PC3 and PC4 are estimated to last for ~230 and ~350 kyr, respectively (Sageman et al., 2006). However, the duration estimate is longer, up to ~870 kyr, in an expanded Tibetan section and the PC2, PC3, PC4 and PC5 were estimated to last for ~50, ~280, ~370, and ~170 kyr, respectively (Li Y X et al., 2017) (Figure 3).

4. Warming magnitudes and rates of the two types of hyperthermal events in the Mesozoic and Cenozoic

4.1 Temperature changes across the NCHE

During the PTB event, the oxygen isotopes of conodont from the Meishan GSSP section in South China (Joachimski et al., 2012) show that: (1) the paleotemperature was ~22°C before the onset of this event (22nd–23rd layers); (2) the paleotemperature rose to 23–27°C in the NC2 stage (24th-26th layers) and to 29–30°C or 33–35°C, as suggested by different conodont genus, in the NC3 stage (27th layer). These results indicate that warming by a conservative estimate of more than 8–10°C (Joachimski et al., 2012) occurred in the NC2 stage (lasting for ~21 kyr, broadly corresponding to the results from the Shangsi section (Sichuan, China) (Cao et al., 2009; Joachimski et al., 2012; Shen et al., 2019). The PTB interval in Sun et al. (2012) further showed that the temperature continued to increase in the NC3 stage, with a magnitude exceeding 14°C. Chen et al. (2016) reconstructed the paleotemperatures of the PTB interval from the Meishan, Shangsi, Daijiagou and Liangfengya sections by SIMS. Their results indicated a rapid warming of approximately 10° Crecorded in the layer equivalent to the 26th layer of the Meishan section, but no obvious temperature changes were observed before the mass extinction and during the extinction maximum.

The TOAE paleotemperature data are mainly based on the brachiopods, bivalves, belemnite and fishbones in the middle-latitudes of western Tethys in England, France, Spain and Portugal. The oxygen isotopes show a rapid negative excursion during the NC2, suggesting that the temperature of shallow seawater in the northern hemisphere increased by ~7–10°C (Dera et al., 2009, 2011; Korte et al., 2015). The warming and negative CIE onset were synchronous. The temperature reached its maximum in NC3 stage, then decreased rapidly by 2–3°C, and showed slight decrease or remained stable in the late NC3 stage (Dera et al., 2009, 2011; Korte et al., 2015).

During the PETM, the warming phase was synchronous with the CIE onset (NC2). In low-latitudes, Sr/Ca and Mg/Ca ratios indicated that the sea surface temperature (SST) increased by 4–5°C in the Pacific equatorial region (Zachos et al., 2003); Oxygen isotopes of planktonic foraminifera indicated an increase in SST of at least 3°C, and the maximum temperature exceeded 40°C in Tanzania of East Africa (Aze et al., 2014). In mid-latitudes, the paleotemperatures inferred from biomarker compounds (MBT-CBT and TEX_{86}) in Gulf of Mexico showed that SST increased by 6–8°C (Sluijs et al., 2014); TEX_{86} and oxygen isotopes of planktonic foraminifera in Wilson Lake indicated that SST increased by at least 8°C with a maximum temperature of 33°C (Zachos et al., 2006). In high-latitudes, TEX_{86} data of ODP site 1772 in the southwestern Pacific indicated that SST increased by ~7° C (Sluijs et al., 2011); Oxygen isotopes of planktonic foraminifera from ODP site 690 in the Southern Ocean indicated that SST increased by ~5–9°C (Thomas et al., 2002); TEX_{86} data from the Arctic Integrated Ocean Drilling Program (IODP) Expedition 302 site suggested that sea surface warming by 5°C (Sluijs et al., 2006). These data together show that SST increased by 3–5°C at low latitudes and 5–9°C at mid- to high-latitudes during the NC2 stage of the PETM, indicating a significant amplification effect in high-latitudes.

4.2 Temperature changes across the PCHE

The SST of the low-latitude Atlantic was ~30–36°C during OAE1a, decreased by ~4°C at the beginning of stage PC3, and then rapidly increased by ~6°C (Dumitrescu and Brassell, 2006). TEX_{86} data from the mid-latitude Atlantic showed a SST increase by ~2–4°C during stage PC2 and a decrease of ~4–6°C during stage PC3 (Naafs and Pancost, 2016). In the mid-latitudes of Boreal area, TEX_{86} and belemnites oxygen isotopes indicated that SST increased by

~3–4°C during stage PC2 (Mutterlose et al., 2010, 2014). In the high-latitudes of the Southern Ocean, SST increased by ~2–3°C during stage PC2 and then cooled with a temperature decrease of 3°C after stage PC3 (Jenkyns et al., 2012).

During the OAE2, SST increased significantly at different latitudes (Gustafsson et al., 2003; O'Brien et al., 2017; Huber et al., 2018). In equatorial Atlantic, oxygen isotopes of planktonic foraminifera and TEX_{86} data indicated that SST increased by ~2–3°C (Forster et al., 2007). In mid-latitude Atlantic, TEX_{86} data showed a rapid cooling of ~4–5°C during stage PC3 and a rapid warming of ~4–5°C during the early phase of stage PC4, with a SST of as high as 34°C (Sinninghe Damsté et al., 2010; Huber et al., 2018). The SST at high latitudes in the northern hemisphere increased by ~7–8°C (Jenkyns et al., 2004), whereas SST increased by ~10°C in the southern hemisphere (Huber et al., 2018). There were also short-term temperature changes during the OAE2 (Forster et al., 2007; O'Brien et al., 2017). A cooling event during OAE2 was observed in Europe that interrupted the overall warming trend (Jenkyns et al., 2017). The cooling event was thought to be mainly due to large-scale burial of organic matter (Jarvis et al., 2006) or enhanced continental weathering (Pogge von Strandmann et al., 2013), which caused the drawdown of atmospheric CO_2 concentration.

4.3 Comparison of the magnitudes and rates of temperature increase

The warming intervals of all these five hyperthermal events were almost synchronous with the onset of CIEs. Therefore, we use the duration of the CIE onset and the magnitude of corresponding temperature increase to calculate warming rates of each event. When calculating rate of warming, duration estimates from GSSP or typical sections were preferentially used and the magnitude of temperature increase is based on the reported data in the literature (Figure 4).

4.3.1 Warming magnitudes and rates of the NCHE

The paleotemperature during the PTB is mainly based on the oxygen isotopes of low latitudes, and its increase (~8–10°C) starts at the onsets and the lower part of the negative CIE plateau. Based on the Meishan GSSP section, the onset duration of the PTB is ~60 kyr (Burgess et al., 2014), and thus the warming rate is ~0.133–0.167°C kyr^{-1}. Paleotemperature data of the TOAE are mainly based on brachiopods, bivalves, arrow stones, and fishbones in middle-latitude regions, suggesting warming of ~7–10°C. The TOAE duration estimated from the Peniche GSSP section is ~150 kyr (Suan et al., 2008b) and thus the warming rate for TOAE is ~0.047–0.067°C kyr^{-1}. Paleotemperature data of the PETM are mainly from foraminifera oxygen isotope and TEX_{86}, and warming occurred during the CIE onset stage, by 3–5, 6–8 and 5–9°C at low-, mid-, high-latitudes. The PC2 duration of the PETM was estimated to be 3–5 kyr (Zeebe et al., 2009; Bowen et al., 2015; Frieling et al., 2017; Turner, 2018), and thus the minimum warming rate is ~0.6–1.0, ~1.2–1.6, 1.0–1.8°C kyr^{-1}, respectively, if the onset duration of 5 kyr is used.

4.3.2 Warming magnitudes and rates of the PCHE

Paleotemperature reconstruction of the OAE1a is mainly based on TEX_{86} data, which show warming at the CIE onset, by ~5–6, ~2–4, and ~2–3°C at low, middle, and high latitudes, respectively. The onset duration of the OAE1a is 75 kyr, which is based on the Yenicesihlar section in Turkey (Hu et al., 2012), and therefore the warming rate in low, middle and high latitudes is ~0.067–0.080, ~0.027–0.053, and ~0.027–0.040°C kyr^{-1}, respectively. Paleotemperature data of the OAE2 are mainly based on oxygen isotopes of planktonic foraminifera and TEX_{86}. The warming of the OAE2 occurred in the CIE onset stage and the magnitude of warming increased from 2–3°C at low latitudes, through, 4–5°C at middle latitudes, to 7–10°C at high latitudes. In this study, we used the PC2 duration of 50 kyr from the Gongzha

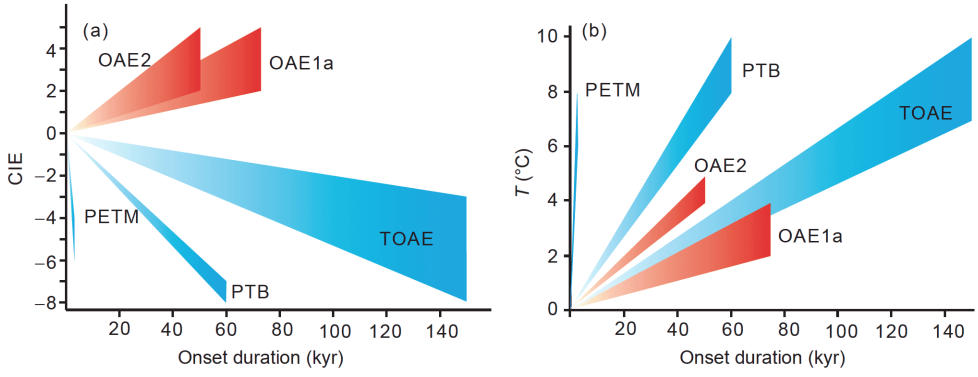

Figure 4 (a) Plots of CIE magnitude versus onset duration of the NCHEs and PCHEs showing the different rates of carbon release; (b) plots of temperature increase versus onset duration of the NCHEs and PCHEs showing the different rates of warming . Warming rate for the PTB is calculated using temperature data from low latitudes. For other events, warming rates are calculated using temperature data from high latitudes and the references are shown in Table 1.

section in southern Tibet (Li Y X et al., 2017) and obtained warming rates of ~0.04–0.06, ~0.08–0.1 and ~0.14–0.2°C kyr^{-1} for the low, middle and high latitudes, respectively.

Among the five hypothermal events, the PTB event exhibited the greatest warming, followed by TOAE, OAE1a, PETM and OAE2 (Figure 4). For the rate of warming, the PETM is the highest (greater than 1°C kyr^{-1}), followed by the PTB, OAE1a, OAE2 and TOAE (Figure 4). In comparison, the rate of modern global warming (1°C in 150 years) is 4.2−5.6 times of that in middle-latitude area during the onset of PETM.

5. Environmental changes caused by the two types of hyperthermal events

5.1 Marine depositional environmental changes across the two types of hyperthermal events

While all the five hyperthermal events are recorded in shallow-marine environment settings, OAE1a, OAE2 and PETM have also been recorded in deep-sea environment settings.

5.1.1 Marine depositional response to the NCHE

(1) Demise of carbonate platforms in shallow-marine environment. Carbonate platform drownings were widely reported related the NCHE (Godet, 2013). For the PTB, the demise of carbonate platforms and the disappearance of laminated siliceous rocks and coals disappeared were accompanied by the emergence of black shale, argillaceous dolomite, pyrite layer, ash clay, and microbialites (Cao and Zheng, 2009). There were also demise of carbonate platforms during the TOAE, where the *Lithiotis* bivalves limestones were replaced by dark-gray spotted and micritic limestones (Sabatino et al., 2013; Han et al., 2016, 2018) or transformed to unfossiliferous, oolitic limestone (Trecalli et al., 2012). During the PETM, the growth of shallow-water carbonate platform was temporarily interrupted by deposition of siliciclastic mudstone in Spain (Pujalte et al., 2014), or channelized conglomerates in southern Tibet (Li J et al., 2017).

(2) Anachronistic deposition in marine environment. The 'anachronistic' sediments widely appeared in the continental margin environment during the PTB including flat-pebble conglomerates, vermicular limestone, microbialites, carbonate seafloor fans, banded limestone, and giant oolitic limestone (Zhao et al., 2008; Li et al., 2010) (Figure 4). During the TOAE, in low-middle latitudes of the Tethys Ocean, intensified storm deposits with erosive surfaces, gutter casts, and hummocky cross stratification structures are present (Krencker et al., 2015; Han et al., 2018; Izumi et al., 2018). In shallow marine environment, an abrupt lithological change from shallow-marine carbonates to channelized conglomerates in southern Tibet (Li J et al., 2017) and to siliciclastic mudstone in Spain are observed during the PETM (Pujalte et al., 2014), while pelagic mudstone was replaced by dark-red clay in deep-sea environment (Zachos et al., 2005).

5.1.2 Marine depositional response to the PCHE

(1) Partial demise of carbonate platform in shallow-marine environment. For the OAE1a, the demise of carbonate platforms was accompanied by the occurrence of a condensed interval and hardgrounds in the northern Tethys margin (Skelton and Gili, 2012), whereas deposition continued and strata rich in *Lithocodium-Bacinella* and or *orbitolinid* are deposited in the southern Tethys margin (Husinec et al., 2012). For OAE2, the demise of carbonate platforms only occurred in the Pyrenees area, northern Spain (Drzewiecki and Simo, 1997), western Croatia (Korbar et al., 2012) and southeastern Turkey (Mülayim et al., 2019).

(2) Organic-rich black shales common in deep-sea environment. The pelagic limestone was replaced by either black shale or organic-rich deposits during both OAE1a and OAE2 (van Bentum et al., 2009; Hu et al., 2012; Patruno et al., 2015; Li et al., 2016).

5.2 Marine environmental changes

Marine environmental response to these hyperthermal events including redox conditions, ocean acidification, and sea level change are examined in this study.

5.2.1 Marine environmental changes caused by the NCHE

(1) Different degree of anoxia occurred in marine environment, but spatial extent of anoxia needs to be better defined. The occurrence of organic-rich black shales, framboidal pyrite, and green sulfur bacteria bloomed indicates anoxic environment during the PTB (Cao et al., 2009). During the TOAE, the northern Europe experienced strong anoxia (Hesselbo et al., 2000), while the southern part was hyoxic or oxic (Hesselbo et al., 2007). The global atmospheric O_2 concentration decreased during the PETM (Harding et al., 2011; Winguth et al., 2012), and the deep-sea was dominated by anoxia or suboxic conditions (Pälike et al., 2014). However, continental shelf and slope environments are characterized by seasonal anoxic or hyoxic conditions (Speijer and Wagner, 2002; Sluijs et al., 2014).

(2) Ocean acidification was widespread, but degree of acidification in shallow marine and deep sea environment needs to be clarified. The timing of ocean acidification during the PTB is controversial. Some studies show that ocean acidification occurred within the onset stage based on carbonate calcium isotopic negative excursion (Payne et al., 2010; Hinojosa et al., 2012), while other studies suggest that ocean acidification occurred within the negative carbon

isotopic plateau stage based on boron isotopic composition (δ^{11}B) (Clarkson et al., 2015). The carbonate calcium isotopic negative excursion during the TOAE indicates ocean acidification (Brazier et al., 2015). During the PETM, the deep-sea environment is characterized by widespread dissolution of deep-sea carbonates that intensified with depth (Zachos et al., 2005). Also, δ^{11}B of planktonic foraminifer shows a decrease and B/Ca ratio of shell declined, indicating a drop in pH of the surface and lysocline (Penman et al., 2014).

(3) Sea level changes are still controversial. Jiang et al. (2014) and Yin et al. (2014) suggested a regression at the onset of the PTB, which is marked by the pyrite layer on the top of bed 24e in Meishan section and/or the dissolution surface at the bottom of microbialites in the Daguizhou beach. However, Cao and Zheng (2009) suggested that this dissolution surface resulted from ocean acidification. A brief regression was detected just before the TOAE onset, and followed by a transgression (Haq, 2018; Krencker et al., 2019). In several instances, an eustatic rise was observed during the PETM, which began 20 to 200 ka before the event with shorelines migrating towards the land (Speijer and Wagner, 2002; Harding et al., 2011; Sluijs et al., 2008). However, in other instances, a regression was observed in the latest Paleocene, followed by a transgression during the PETM (Schmitz and Pujalte, 2003, 2007; Pujalte et al., 2014).

5.2.2 Marine environmental response to the PCHE

(1) Redox conditions were not uniform, and varied spatially and temporally. For example, anoxic conditions were observed in deep settings of the Western Tethys, whereas the shallow-water and continental margin environments were dominated by hyoxic or oxic conditions during the OAE1a (Westermann et al., 2013). The deep proto-North Atlantic experienced anoxia and euxinia during the OAE2 (Pancost et al., 2004) and its southern part showed more severe anoxia and euxinia (van Bentum et al., 2009; van Helmond et al., 2014). In equatorial Atlantic, anoxic conditions are found to alternate between ferrigenous and euxinic in Demera Rise and in the Moroccan shelf (van Bentum et al., 2009). Northern and middle latitudes of the proto-North Atlantic also documented a brief episode of oxygenation punctuating the major anoxia during the OAE2 (van Helmond et al., 2014; Goldberg et al., 2016).

(2) The oceanic currents may be reorganized. Nd isotopes have been used to track oceanic flow patterns. Fish debris from ODP site 1258 in North Atlantic exhibits a dramatic positive excursion of 8ε_{Nd} units during OAE2 (MacLeod et al., 2008), and the fish debris from the Eastbourne section in the UK shows a negative excursion of 1ε_{Nd} units, followed by a positive excursion of 3ε_{Nd} units during the OAE2 (Zheng et al., 2013).

(3) Ocean acidification and sea level changes across the PCHEs were still unclear. Eustatic sea level changes were observed during the Turonian hot greenhouse climate (Haq and Huber, 2017).

5.3 Changes in terrestrial environment

5.3.1 Terrestrial environmental response to the NCHEs

(1) Extreme droughts were widespread in terrestrial environment. Red sediments occurred widely in northern China with decreasing coal accumulation and increasing heat- and drought-tolerant plants during the TOAE (Deng et al., 2012). A distinct shift to drier soils occurred just prior to the PETM, and continued until the PETM recovery stage, followed by wetter conditions (Wing et al., 2005; Kraus and Riggins, 2007).

(2) Enhanced hydrological cycle and altered river morphology. The PTB was characterized by a rapid and apparently basin-wide change from meandering to braided river systems, as evidenced by preserved sedimentary facies (Ward et al., 2000; Shen et al., 2011; Zhu et al., 2019). Water discharge increased by at least 1.35 times and potentially up to 14 times during the early phase of the PETM in northern Spain where an abrupt transition from overbank palaeosol deposits to conglomeratic fluvial sequence, indicating extreme floods, quick channel mobility and increase of channel dimensions (Chen et al., 2018). Stratigraphic intervals at the main part of the PETM in northern Bighorn basin correspond to thick paleosols and thin avulsion deposits, and the anomalously thick channel-belt sandstone, while stratigraphic intervals below and above the main part of the PETM correspond to thinner paleosols and thick avulsion deposits (Kraus et al., 2015).

5.3.2 Terrestrial depositional response to the PCHEs

The impacts of the PCHEs on terrestrial environment are not well known, mainly because there are few of terrestrial records. In lakes, increases in nutrient input and primary productivity led to anoxia or seasonal anoxia with deposition of organic rich black shales (Jenkyns, 2010). Arid and humid conditions were not uniform, and varied spatially and temporally. For example, the Changma Basin in China documents a humid condition with seasonal aridity (Suarez et al., 2017), while the Utah foreland basin in North America documents an arid climate during OAE1a (Ludvigson et al., 2010).

6. Biotic changes caused by NCHE and PCHE

Statistical analysis reveals that the family-level extinction rates across the PTB, TOAE and PETM of NCHE, and OAE1a and OAE2 of PCHE are 55.7%, 17.3%, 7.6%, 9.9%

and 13.6% (Sepkoski, 1996), respectively. The PTB, TOAE, and OAE2 events were three of the eighteen largest biotic crises in the Phanerozoic (Bambach, 2006). The NCHEs have more significant impacts on biota than the PCHEs, except for the PETM that is likely related to the short duration of warming.

6.1 Biotic changes caused by the NCHE

6.1.1 Marine biotic changes

(1) Migration from low to higher latitudes. Most marine biota was affected including ammonites, foraminifera, ostracods, and belemnites and migrated poleward across the TOAE and PTB (Dera et al., 2011; Bernardi et al., 2018). In the Tethys Ocean, the shallow platform organisms at low to middle latitudes show a gradual replacement from reef-building corals, to large benthic foraminifera during the PETM, and the coral reefs migrated from low latitudes to higher middle latitudes (Scheibner and Speijer, 2008).

(2) Extinctions or/and turnover were widespread in marine biota, but varied in extent. In several instances, biota were sensitive to marine environmental changes including temperature, $[O_2]$ and pH often experienced extinction or/and turnover. Calcareous algae, fusulinids, rugose corals, tabulate corals, trilobites and radiolarians were entirely lost in the latest Permian (Shen and Zhang, 2017). Small foraminifers, ostracods, brachiopods, bivalves, gastropods, ammonoids and conodonts seems to be less affected by this end-Permian mass extinction (Song et al., 2013). The shallow platform *Lithiotis* bivalves experienced extinction at the low latitudes of the southern margin of Tethys during the early Toarcian (Trecalli et al., 2012; Sabatino et al., 2013). In deep-sea environment, the extinction rates are 30% in small benthic foraminifera (Takeda and Kaiho, 2007) and up to 18 species appeared or disappeared in calcareous nannofossils across the PETM (Gibbs et al., 2006). Late Paleocene larger-foraminifera assemblages represented by *Ranikothalia* and *Miscellanea* were replaced by early Eocene taxa represented by *Nummulites* and *Alveolina* in shallow marine carbonate platform (Scheibner et al., 2005).

(3) Altered biotic morphology and species abundance. The size of most marine biota decreased including small foraminifers, bivalves, gastropods, brachiopods, ostracods, conodonts and fish, while cyanobacteria boomed during the PTB (Wilson and MacArthur, 1967). The TOAE coincided with size reductions in microplankton and molluscan shells (Morten and Twitchett, 2009). *Apectodinium* bloomed during and shortly before the PETM and shows variations in abundance (Sluijs and Brinkhuis, 2009). An unusual increase in the size of surface-water planktonic in contrast to deep-water benthic foraminifera which decreased in size during the PETM (Kaiho et al., 2006).

6.1.2 Terrestrial biotic changes

(1) Migration from low to higher latitudes. Thermophilic and drought-tolerant plants increased and immigrated to the higher latitudes across the TOAE (Deng et al., 2012). The conifers and broad-leaved lineages were replaced by bean family in Bighorn basins of North America, which immigrated 650–1500 km from southern latitudes during the PETM (Wing et al., 2005), accompanied by the disperse of new mammals and lizards (McInerney and Wing, 2011).

(2) Extinctions or/and blooms were widespread in continental biota. The tropical rainforests represented by Gigantopteris flora disappeared in South China, (Shen et al., 2011; Yu et al., 2015; Bernardi et al., 2018), and *Dicynodon* that dominated the latest Permian was replaced by *Lystrosaurus* at the earliest Triassic (Ward et al., 2005; Gastaldo et al., 2019). The Champsosaurus and Plesiadapidae disappeared, while *Perissodactyla*, *Artiodactyla*, rodents and primates bloomed across the PETM (Gingerich, 2003).

6.2 Biotic changes caused by the PCHE

The effects of the PCHE on the terrestrial and shallow-marine biota are negligible, but were much more significant on the deep-sea biota. Biota sensitive to marine environmental changes often experienced extinction or/and turnover such as the nanoconid crisis across the OAE1a (Erba et al., 2010). Some *Rotalipora* genus experienced significant extinction, while some *Heterohelix* genus showed proliferation across the OAE2 (Leckie et al., 2002; Erba, 2004). Radiolaria experienced significant extinction during both the OAE1a and OAE2, and the extinction rates were 41% and 58%, respectively (Erbacher et al., 1996).

7. Driving mechanisms of the two types of hyperthermal events

7.1 Driving mechanisms of the NCHE

The NCHE are characterized by a negative carbon isotopic excursion, which resulted from volcanic eruption associated with the formation of continental LIPs (Figure 5a).

(1) Strong temporal association between LIP volcanism and NCHE and a causal link between the two phenomena are indicated by proxy evidence for volcanism in stratigraphic horizons recording the onset of environmental change. The PTB, TOAE and PETM were associated with end-Permian Siberian Traps, Pliensbachian-Toarcian Karoo-Ferrar Province, and North Atlantic Igneous Province, respectively (Wignall, 2001; McElwain et al., 2005; Bond and Wignall, 2014; Burgess et al., 2015, 2017; Ernst and Youbi, 2017). All these LIPs associated with the NCHE are of continental nature. That is the volcanism was predominantly subaerial

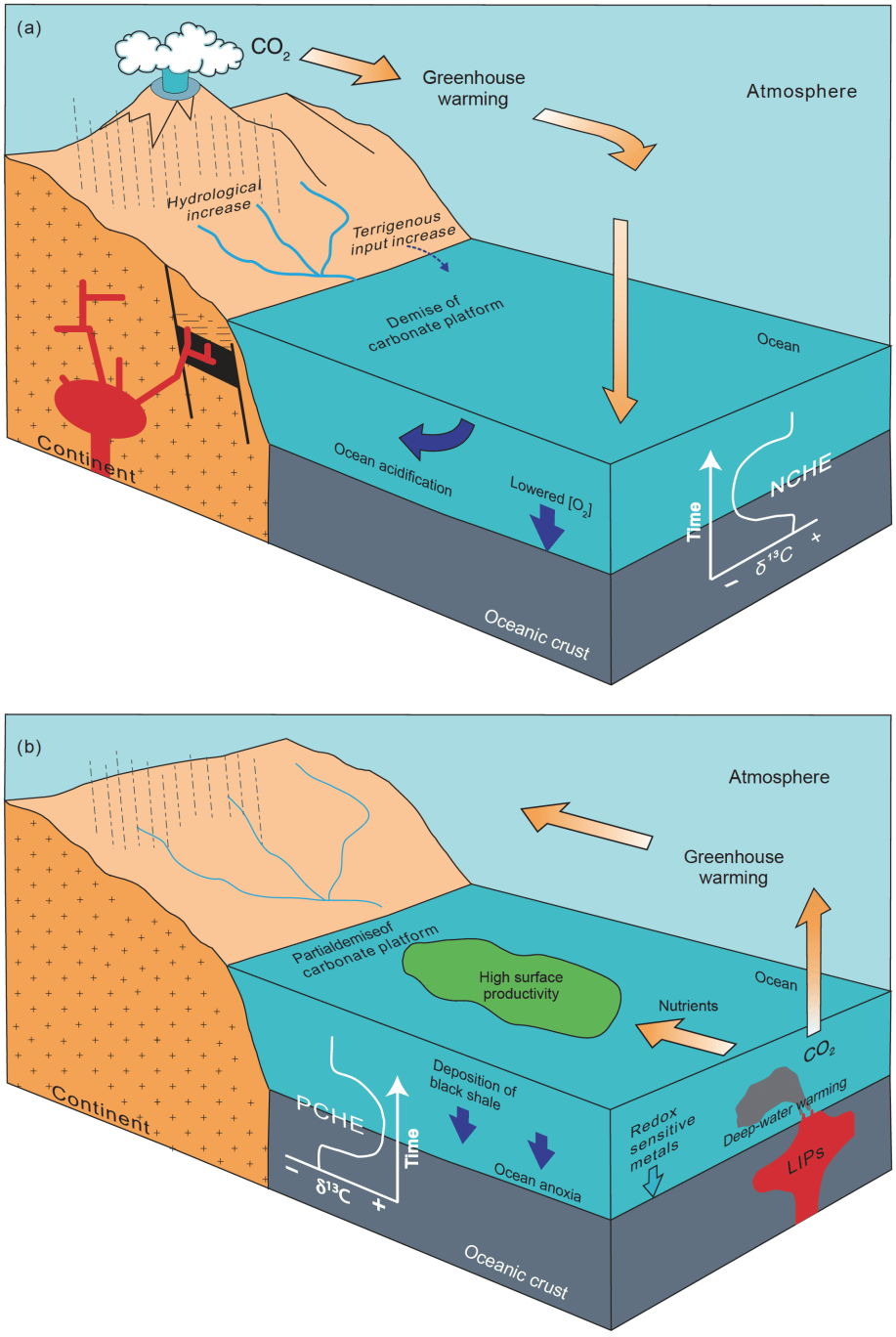

Figure 5 Driving mechanisms and environmental impacts of the NCHEs and PCHEs (modified from Robinson et al, 2017). (a) The NCHEs were driven by terrestrial LIPs causing the increase of terrestrial and nutrient input, the demise of shallow-water carbonate platform and lowered O_2 content; (b) the PCHEs were driven by submarine LIPs causing high surface productivity, partial demise of shallow-water carbonate platform, anoxia and deposition of black shale.

(Continental Flood Basalts).

(2) Sources of carbon released during the NCHE are highly uncertain and have been proposed to be related to methane hydrates, massive flood basalts, and sill emplacement. Magmatic emissions and thermogenic volatiles resulting from intruded volatile-rich sediments such as organic-rich shales, coals, and evaporates by LIP magmas may explain the observed negative carbon-isotope excursions (Gutjahr et al., 2017).

(3) The eruption of continental LIPs resulted in distinct changes of temperature, environment and biota in both marine and continental environments. The effects on atmospheric and continental environments include global warming, increase of wildfires and droughts, intensified

continental weathering and terrigenous input, acid rain, ozone layer destruction (Ernst and Youbi, 2017). Impacts on non-marine environments include the demise of carbonate platforms, ocean acidification, oceanic anoxia, as well as the extinction, turnover and migration of marine biota (Rong and Huang, 2014; Song and Tong, 2016; Bond and Grasby, 2017; Shen and Zhang, 2017; Benton, 2018).

7.2 Driving mechanisms of the PCHE

The PCHE are characterized by a positive carbon isotopic excursion, which resulted from the submarine volcanic eruption associated with the formation of LIPs (Figure 5b).

(1) Strong temporal association between LIP volcanism and PCHE and a causal link between the two phenomena are indicated by proxy evidence for volcanism in stratigraphic horizons recording the onset of environmental change. OAE1a was associated with the Ontong Java Plateau and OAE2 was associated with four LIPs including the Caribbean-Columbian Plateau, the High Arctic LIP, the Ontong-Java Plateau, and the Madagascan Province (Wignall, 2001; Ernst and Youbi, 2017). All these LIPs associated with the PCHE are Oceanic Plateau, where volcanism occurred predominantly below the sea surface.

(2) Sources of carbon released during the PCHE have been proposed to be related to massive flood basalts. Initial magmatic emission caused increase in atmospheric pCO_2, leading to the initial negative carbon-isotope excursion, global warming, intensification of continental weathering, and enhanced delivery of nutrients to oceans. This weathering-derived magmatic and emissions stimulation of ocean export productivity combined with decreased O_2 delivery to deep ocean as a result of solubility-temperature relationships to further reduce oxygen content in deep water. Abundant organic matter was buried as a result of oceanic anoxia, causing the observed positive carbon-isotope excursions.

(3) The effects of submarine LIPs eruption on environment include widespread anoxia, large-scale burial of organic matter, and partial demise of carbonate platform. The effects on the continental and shallow-marine biota are negligible, but were much more severe on the deep-sea biota such as the nanoconid crisis across the OAE1a (Erba et al., 2010).

8. Implications for identifying driving mechanisms of other hyperthermal events

Based on previous studies of the above five hypothermal events, we infer that the Triassic-Jurassic boundary event (~201 Ma), which was associated with CAMP LIP, and the Cretaceous-Paleogene boundary event (~66 Ma), which was related to Deccan LIP, belong to the NCHEs and were likely caused by terrestrial LIPs. Similarly, the early Cretaceous Valanginian oceanic anoxic event (~132 Ma), which was associated with Parana-Etendeka and Bunbury-Comei LIPs (Appendix Table S1, https://link.springer.com), belongs to the PCHE and was likely caused by marine LIPs. Well preserved magmatic records of these hyperthermal events allow us to link the LIP volcanism with onset of environmental change. For details of these hyperthermal events, readers are referred to the related literature. On the other hand, as we know, LIPs prior to the late Jurassic are not well preserved as a result of plate subduction. Most of these LIPs disappeared or/and are preserved sporadically. Thus, it has been very difficult to link the LIP volcanism and the major environmental changes before the Late Jurassic. The findings of this study allow us to deduce driving mechanisms of major geological events if the type of these events can be classified based on the sedimentation, environmental, carbon isotopic, and biotic records. Three examples are given below to show the applications of the findings of this study.

Case study 1. The Carnian Pluvial Event (~234–232 Ma, CPE). The CPE is characterized by ~6–8°C warming and a negative carbon excursion of −4.2‰ in South China and Oman (Dal Corso et al., 2012; Sun et al., 2019). The effects on environment include a distinct shift to more humid conditions, an increase in precipitation and terrigenous input, and the temporary demise of carbonate platform (Simms and Ruffell, 1989; Jin et al., 2015). Terrestrial plants and shallow-marine invertebrates experienced varying extinction or/and replacement. For example, high extinction rates of ammonites and crinoids, and a dramatic increase in conifers are recorded. The first known dinosaurs and calcareous planktons occurred shortly after the CPE. Thus, we infer that the CPE belongs to the NCHE and was driven by continental LIPs. The CPE has been linked to Wrangellia flood basalts which are exposed in Alaska, Yukon and British Columbia. The Wrangellia flood basalt overlies black shales with middle to Ladinian *Daonella* and is overlain by middle to late Norian shallow marine carbonates. Thus, the eruptions of the Wrangellia flood basalts occurred in a submarine environment (Stanley, 1989), supporting our inference mentioned above.

Case study 2. The early mid-Cambrian Event (~510 Ma). This event is characterized by a negative carbon isotopic excursion, a positive sulfur isotopic excursion, a sea level rise (Montañez et al., 2000; Hough et al., 2006), widespread anoxic conditions (Zhuravlev and Wood, 1996), and a significant biotic extinction (Sepkoski, 1996). Thus, we infer that this event belongs to the NCHE and was related to continental LIPs. Recently, the eruptions of Kalkarindji LIP in western Australia was dated at 510.7±0.6 Ma (Jourdan et al., 2014), and coincided with the onset of the early mid-Cambrian Event, suggesting that a causal relationship might exist. The eruption of Kalkarindji LIP occurred in a continental environment (Jourdan et al., 2014), supporting the

mentioned inference.

Case study 3. The Frasnian-Famennian Event (~372 Ma, F/F). The F/F event is characterized by a ~9°C warming, a 3.0‰ positive carbon excursion (Joachimski et al., 2002, 2009; Xu et al., 2012), anoxic conditions, and widespread deposition of black shale (Murphy et al., 2000). The F/F event is one of the five largest biotic crises of the Phanerozoic and its impacts on low latitudes and shallow marine biota were much more severe than that on high latitudes and continental biota. Although multiple episodes of mercury enrichment are reported to indicate volcanic eruption (Racki et al., 2018), no large-scale volcanic rocks are observed across the F/F event. According to its sedimentation, environmental, carbon isotopic, and biotic characteristics, we infer that the F/F event belongs to the PCHE and was likely caused by submarine LIPs. Further studies of the inferred link is required.

9. Conclusions and perspective

This study provides systematic review and summary of sedimentation, environmental, carbon isotopic, and biotic characteristics of five major hyperthermal events in the Mesozoic and Cenozoic and obtains interesting quantitative measures of these hyperthermal events, which provide an important basis for understanding global warming and constraining the driving mechanisms of the hyperthermal events. The main conclusions are as follows:

(1) The hyperthermal events are classified into two types based on carbon isotope profiles of these event: the negative carbon isotopic excursion hyperthermal Event, NCHE, and the positive carbon isotopic excursion hyperthermal event, PCHE. The NCHE include the PTB, TOAE and PETM, and was caused by continental LIPs. The PCHE include OAE1a and OAE2, was driven by submarine LIPs.

(2) The negative CIE of the NCHE was related to large-scale injection of light carbo into the ocean-atmosphere systems. Their effects on environment include global warming, increase of wildfires and droughts, intensified continental weathering and terrigenous input, the demise of carbonate platforms, ocean acidification and oceanic anoxia, and the extinction, turnover and migration of marine biota.

(3) The PCHE resulted from large-scale burial of organic matter. The effects on environment include widespread anoxia, deposition of black shale and partial demise of carbonate platform. The effects on the continental and shallow-marine biota were negligible, but were much more severe on the deep-sea biota.

The past can be the key to the future. Studying deep-time hyperthermal events provides an important reference for understanding the current global warming. In 2017, a special topic "Cretaceous greenhouse paleoclimate and sea-level changes" was published in *Science China Earth Sciences* (Hu et al., 2017). This special issue focused on the Cretaceous greenhouse climate and sea level change. In 2018, the Royal Society of UK organized a seminar "Hyperthermals: rapid and extreme global warming in our geological past" with 11 thematic articles (Foster et al., 2018). All these studies focused on greenhouse climate and hyperthermal events. Our understanding of past hyperthermal events is impeded by incomplete geological records and imprecise or inaccurate climate-environment parameters, but it can be improved by collecting more accurate and reliable data. Understanding past climate, especially hyperthermal events, has important theoretical and practical significance for understanding both the past and the future (Wang et al., 2017).

Acknowledgements *We thank Chengshan WANG, Zhengtang GUO Shuzhong SHEN, David KEMP, Micha RUHL, Ying CUI, Chunju HUANG and Jitao CHEN for their constructive discussions and useful suggestions. We are grateful to six anonymous reviewers and associate editor Jianfang HU for their comments that greatly helped to improve the manuscript. This study was financially supported by the National Natural Science Foundation of China (Grant No. 41888101) and National Natural Science Fund for Distinguished Young Scholars (Grant No. 41525007).*

References

Aze T, Pearson P N, Dickson A J, Badger M P S, Bown P R, Pancost R D, Gibbs S J, Huber B T, Leng M J, Coe A L, Cohen A S, Foster G L. 2014. Extreme warming of tropical waters during the Paleocene-Eocene thermal Maximum. Geology, 42: 739–742

Aziz H A, Hilgen F J, van Luijk G M, Sluijs A, Kraus M J, Pares J M, Gingerich P D. 2008. Astronomical climate control on paleosol stacking patterns in the upper Paleocene-lower Eocene Willwood Formation, Bighorn Basin, Wyoming. Geology, 36: 531–534

Bains S, Corfield R M, Norris R D. 1999. Mechanisms of climate warming at the end of the Paleocene. Science, 285: 724–727

Bambach R K. 2006. Phanerozoic biodiversity Mass extinctions. Annu Rev Earth Planet Sci, 34: 127–155

Benton M J. 2018. Hyperthermal-driven Mass extinctions: Killing models during the Permian-TriassicMass extinction. Phil Trans R Soc A, 376: 20170076

Bernardi M, Petti F M, Benton M J. 2018. Tetrapod distribution and temperature rise during the Permian-Triassic Mass extinction. Proc R Soc B, 285: 20172331

Bond D P, Wignall P B. 2014. Large igneous provinces and Mass extinctions: An update. In: Keller G, Kerr A C, eds. Volcanism, Impacts and Mass Extinctions: Causes and Effects. Spec Pap Geol Soc Am, 505: 29–55

Bond D P G, Grasby S E. 2017. On the causes of Mass extinctions. Palaeogeogr Palaeoclimatol Palaeoecol, 478: 3–29

Bottini C, Cohen A S, Erba E, Jenkyns H C, Coe A L. 2012. Osmium-isotope evidence for volcanism, weathering, and ocean mixing during the early Aptian OAE 1a. Geology, 40: 583–586

Boulila S, Galbrun B, Huret E, Hinnov L A, Rouget I, Gardin S, Bartolini A. 2014. Astronomical calibration of the Toarcian Stage: Implications for sequence stratigraphy and duration of the early Toarcian OAE. Earth Planet Sci Lett, 386: 98–111

Bowen G J, Maibauer B J, Kraus M J, Röhl U, Westerhold T, Steimke A, Gingerich P D, Wing S L, Clyde W C. 2015. Two Massive, rapid releases of carbon during the onset of the Palaeocene-Eocene thermal Maximum. Nat Geosci, 8: 44–47

Brand U, Jiang G, Azmy K, Bishop J, Montañez I P. 2012. Diagenetic

evaluation of a Pennsylvanian carbonate succession (Bird Spring Formation, Arrow Canyon, Nevada, U.S.A.)—1: Brachiopod and whole rock comparison. Chem Geol, 308: 26–39
Brazier J M, Suan G, Tacail T, Simon L, Martin J E, Mattioli E, Balter V. 2015. Calcium isotope evidence for dramatic increase of continental weathering during the Toarcian oceanic anoxic event (Early Jurassic). Earth Planet Sci Lett, 411: 164–176
Burgess S D, Bowring S, Shen S. 2014. High-precision timeline for Earth's most severe extinction. Proc Natl Acad Sci USA, 111: 3316–3321
Burgess S D, Bowring S A, Fleming T H, Elliot D H. 2015. High-precision geochronology links the Ferrar large igneous province with early-Jurassic ocean anoxia and biotic crisis. Earth Planet Sci Lett, 415: 90–99
Burgess S D, Muirhead J D, Bowring S A. 2017. Initial pulse of Siberian Traps sills as the trigger of the end-Permian Mass extinction. Nat Commun, 8: 164
Cao C, Love G D, Hays L E, Wang W, Shen S, Summons R E. 2009. Biogeochemical evidence for euxinic oceans and ecological disturbance presaging the end-Permian Mass extinction event. Earth Planet Sci Lett, 281: 188–201
Cao C Q, Zheng Q F. 2009. Geological event sequences of the Permian-Triassic transition recorded in the microfacies in Meishan section. Sci China Ser D-Earth Sci, 52: 1529–1536
Charles A J, Condon D J, Harding I C, Pälike H, Marshall J E A, Cui Y, Kump L, Croudace I W. 2011. Constraints on the numerical age of the Paleocene-Eocene boundary. Geochem Geophys Geosyst, 12: Q0AA17
Chen C, Guerit L, Foreman B Z, Hassenruck-Gudipati H J, Adatte T, Honegger L, Perret M, Sluijs A, Castelltort S. 2018. Estimating regional flood discharge during Palaeocene-Eocene global warming. Sci Rep, 8: 13391
Chen J, Shen S, Li X, Xu Y, Joachimski M M, Bowring S A, Erwin D H, Yuan D, Chen B, Zhang H, Wang Y, Cao C, Zheng Q, Mu L. 2016. High-resolution SIMS oxygen isotope analysis on conodont apatite from South China and implications for the end-Permian Mass extinction. Palaeogeogr Palaeoclimatol Palaeoecol, 448: 26–38
Clarkson M O, Kasemann S A, Wood R A, Lenton T M, Daines S J, Richoz S, Ohnemueller F, Meixner A, Poulton S W, Tipper E T. 2015. Ocean acidification and the Permo-Triassic Mass extinction. Science, 348: 229–232
Cui Y, Kump L R. 2015. Global warming and the end-Permian extinction event: Proxy and modeling perspectives. Earth-Sci Rev, 149: 5–22
Dal Corso J, Mietto P, Newton R J, Pancost R D, Preto N, Roghi G, Wignall P B. 2012. Discovery of aMajor negative $\delta^{13}C$ spike in the Carnian (Late Triassic) linked to the eruption of Wrangellia flood basalts. Geology, 40: 79–82
Deng S, Li Y, Fan R, Fang L, Li X, Liu L. 2012. Toarcian (Early Jurassic) Oceanic Anoxic Event and the reponse in terrestrial ecological system (in Chinese). Earth Science—J China Univ Geosci, 37: 23–38
Dera G, Neige P, Dommergues J L, Brayard A. 2011. Ammonite paleobiogeography during the Pliensbachian-Toarcian crisis (Early Jurassic) reflecting paleoclimate, eustasy, and extinctions. Glob Planet Change, 78: 92–105
Dera G, Pucéat E, Pellenard P, Neige P, Delsate D, Joachimski M M, Reisberg L, Martinez M. 2009. Water Mass exchange and variations in seawater temperature in the NW Tethys during the Early Jurassic: Evidence from neodymium and oxygen isotopes of fish teeth and belemnites. Earth Planet Sci Lett, 286: 198–207
Drzewiecki P A, Simo J A. 1997. Carbonate platform drowning and oceanic anoxic events on a Mid-Cretaceous carbonate platform, south-central Pyrenees, Spain. J Sediment Res, 67: 698–714
Dumitrescu M, Brassell S C. 2006. Compositional and isotopic characteristics of organic Matter for the early Aptian oceanic anoxic event at Shatsky Rise, ODP leg 198. Palaeogeogr Palaeoclimatol Palaeoecol, 235: 168–191
Erba E. 2004. Calcareous nannofossils and Mesozoic oceanic anoxic events. Mar Micropaleontol, 52: 85–106
Erba E, Bottini C, Weissert H J, Keller C E. 2010. Calcareous nannoplankton response to surface-water acidification around Oceanic Anoxic Event 1a. Science, 329: 428–432
Erbacher J, Thurow J, Littke R. 1996. Evolution patterns of radiolaria and organicMatter variations: A new approach to identify sea-level changes in mid-Cretaceous pelagic environments. Geology, 24: 499–502
Ernst R E, Youbi N. 2017. How Large Igneous Provinces affect global climate, sometimes cause Mass extinctions, and represent naturalMarkers in the geological record. Palaeogeogr Palaeoclimatol Palaeoecol, 478: 30–52
Farley K A, Eltgroth S F. 2003. An alternative age model for the Paleocene-Eocene thermal Maximum using extraterrestrial ^{3}He. Earth Planet Sci Lett, 208: 135–148
Forster A, Schouten S, Moriya K, Wilson P A, Sinninghe Damsté J S. 2007. Tropical warming and intermittent cooling during the Cenomanian/Turonian oceanic anoxic event 2: Sea surface temperature records from the equatorial Atlantic. Paleoceanography, 22: PA1219
Foster G L, Hull P, Lunt D J, Zachos J C. 2018. Placing our current 'hyperthermal' in the context of rapid climate change in our geological past. Phil Trans R Soc A, 376: 20170086
Frieling J, Gebhardt H, Huber M, Adekeye O A, Akande S O, Reichart G J, Middelburg J J, Schouten S, Sluijs A. 2017. Extreme warmth and heat-stressed plankton in the tropics during the Paleocene-Eocene Thermal Maximum. Sci Adv, 3: e1600891
Gastaldo R A, Neveling J, Geissman J W, Li J. 2019. A multidisciplinary approach to review the vertical and lateral facies relationships of the purported vertebrate-defined terrestrial Permian-Triassic boundary interval at Bethulie, Karoo Basin, South Africa. Earth-Sci Rev, 189: 220–243
Gibbs S J, Bown P R, Sessa J A, Bralower T J, Wilson P A. 2006. Nannoplankton extinction and origination across the Paleocene-Eocene thermal Maximum. Science, 314: 1770–1773
Gingerich P D. 2003. Mammalian responses to climate change at the Paleocene-Eocene boundary: Polecat Bench record in the northern Bighorn Basin, Wyoming. Special Papers, 369: 463–478
Godet A. 2013. Drowning unconformities: Palaeoenvironmental significance and involvement of global processes. Sediment Geol, 293: 45–66
Goldberg T, Poulton S W, Wagner T, Kolonic S F, Rehkämper M. 2016. Molybdenum drawdown during Cretaceous oceanic anoxic event 2. Earth Planet Sci Lett, 440: 81–91
Gustafsson M, Holbourn A, Kuhnt W. 2003. Changes in Northeast Atlantic temperature and carbon flux during the Cenomanian/Turonian paleoceanographic event: The Goban Spur stable isotope record. Palaeogeogr Palaeoclimatol Palaeoecol, 201: 51–66
Gutjahr M, Ridgwell A, Sexton P F, Anagnostou E, Pearson P N, Pälike H, Norris R D, Thomas E, Foster G L. 2017. Very large release of mostly volcanic carbon during the Palaeocene-Eocene Thermal Maximum. Nature, 548: 573–577
Han Z, Hu X, Kemp D B, Li J. 2018. Carbonate-platform response to the Toarcian Oceanic Anoxic Event in the southern hemisphere: Implications for climatic change and biotic platform demise. Earth Planet Sci Lett, 489: 59–71
Han Z, Hu X M, Li J, Garzanti E. 2016. Jurassic carbonate microfacies and relative sea-level changes in the Tethys Himalaya (southern Tibet). Palaeogeogr Palaeoclimatol Palaeoecol, 456: 1–20
Haq B. 2018. Triassic eustatic variations reexamined. GSA Today, 28: 4–9
Haq B U, Huber B T. 2017. Anatomy of a eustatic event during the Turonian (Late Cretaceous) hot greenhouse climate. Sci China Earth Sci, 60: 20–29
Harding I C, Charles A J, Marshall J E A, Pälike H, Roberts A P, Wilson P A, Jarvis E, Thorne R, Morris E, Moremon R, Pearce R B, Akbari S. 2011. Sea-level and salinity fluctuations during the Paleocene-Eocene thermal Maximum in Arctic Spitsbergen. Earth Planet Sci Lett, 303: 97–107
Hesselbo S P, Gröcke D R, Jenkyns H C, Bjerrum C J, Farrimond P, Morgans Bell H S, Green O R. 2000. Massive dissociation of gas hydrate during a Jurassic oceanic anoxic event. Nature, 406: 392–395
Hesselbo S P, Jenkyns H C, Duarte L V, Oliveira L C V. 2007. Carbon-

isotope record of the Early Jurassic (Toarcian) Oceanic Anoxic Event from fossil wood andMarine carbonate (Lusitanian Basin, Portugal). Earth Planet Sci Lett, 253: 455–470
Hinojosa J L, Brown S T, Chen J, DePaolo D J, Paytan A, Shen S, Payne J L. 2012. Evidence for end-Permian ocean acidification from calcium isotopes in biogenic apatite. Geology, 40: 743–746
Hough M L, Shields G A, Evins L Z, Strauss H, Henderson R A, Mackenzie S. 2006. AMajor sulphur isotope event at c 510 Ma: A possible anoxia-extinction-volcanism connection during the Early-Middle Cambrian transition? Terra Nova, 18: 257–263
Hu X M, Wagreich M, Sames B. 2017. Special Topic: Cretaceous greenhouse palaeoclimate and sea-level changes. Sci China Earth Sci, 60: 1–4
Hu X M, Wagreich M, Yilmaz I O. 2012. Marine rapid environmental/climatic change in the Cretaceous greenhouse world. Cretac Res, 38: 1–6
Huang C J, Hesselbo S P. 2014. Pacing of the Toarcian Oceanic Anoxic Event (Early Jurassic) from astronomical correlation of Marine sections. Gondwana Res, 25: 1348–1356
Huber B T, MacLeod K G, Watkins D K, Coffin M F. 2018. The rise and fall of the Cretaceous Hot Greenhouse climate. Glob Planet Change, 167: 1–23
Husinec A, Harman C A, Regan S P, Mosher D A, Sweeney R J, Read J F. 2012. Sequence development influenced by intermittent cooling events in the Cretaceous Aptian greenhouse, Adriatic platform, Croatia. AAPG Bull, 96: 2215–2244
Izumi K, Kemp D B, Itamiya S, Inui M. 2018. Sedimentary evidence for enhanced hydrological cycling in response to rapid carbon release during the early Toarcian oceanic anoxic event. Earth Planet Sci Lett, 481: 162–170
Intergovernmental Panel on Climate Change (IPCC). 2018. Special report of global warming of 1.5°C. https://www.ipcc.ch/sr15/
Jarvis I, Gale A S, Jenkyns H C, Pearce M A. 2006. Secular variation in Late Cretaceous carbon isotopes: A new δ^{13}C carbonate reference curve for the Cenomanian-Campanian (99.6–70.6 Ma). Geol Mag, 143: 561–608
Jenkyns H C. 2010. Geochemistry of oceanic anoxic events. Geochem Geophys Geosyst, 11: 1–30
Jenkyns H C, Dickson A J, Ruhl M, Van Den Boorn S H J M. 2017. Basalt-seawater interaction, the Plenus Cold Event, enhanced weathering and geochemical change: Deconstructing Oceanic Anoxic Event 2 (Cenomanian–Turonian, Late Cretaceous). Sedimentology, 64: 16–43
Jenkyns H C, Forster A, Schouten S, Sinninghe Damsté J S. 2004. High temperatures in the Late Cretaceous Arctic Ocean. Nature, 432: 888–892
Jenkyns H C, Schouten-Huibers L, Schouten S, Sinninghe Damsté J S. 2012. Warm Middle Jurassic-Early Cretaceous high-latitude sea-surface temperatures from the Southern Ocean. Clim Past, 8: 215–226
Jiang H, Lai X, Sun Y, Wignall P B, Liu J, Yan C. 2014. Permian-Triassic conodonts from Dajiang (Guizhou, South China) and their implication for the age of microbialite deposition in the aftermath of the End-Permian Mass extinction. J Earth Sci, 25: 413–430
Jin X, Shi Z, Wang Y, et al. 2015. Mid-Carnian (Late Triassic) extreme climate event: Advances and unsolved problems (in Chinese). Acta Sedimentol Sin, 33: 105–115
Joachimski M M, Breisig S, Buggisch W, Talent J A, Mawson R, Gereke M, Morrow J R, Day J, Weddige K. 2009. Devonian climate and reef evolution: Insights from oxygen isotopes in apatite. Earth Planet Sci Lett, 284: 599–609
Joachimski M M, Pancost R D, Freeman K H, Ostertag-Henning C, Buggisch W. 2002. Carbon isotope geochemistry of the Frasnian-Famennian transition. Palaeogeogr Palaeoclimatol Palaeoecol, 181: 91–109
Joachimski M M, Lai X, Shen S, Jiang H, Luo G, Chen B, Chen J, Sun Y. 2012. Climate warming in the latest Permian and the Permian-Triassic Mass extinction. Geology, 40: 195–198
Jones T D, Lunt D J, Schmidt D N, Ridgwell A, Sluijs A, Valdes P J, Maslin M. 2013. Climate model and proxy data constraints on ocean warming across the Paleocene-Eocene Thermal Maximum. Earth-Sci Rev, 125: 123–145
Jourdan F, Hodges K, Sell B, Schaltegger U, Wingate M T D, Evins L Z, Söderlund U, Haines P W, Phillips D, Blenkinsop T. 2014. High-precision dating of the Kalkarindji large igneous province, Australia, and synchrony with the Early-Middle Cambrian (Stage 4–5) extinction. Geology, 42: 543–546
Kaiho K, Takeda K, Petrizzo M R, Zachos J C. 2006. Anomalous shifts in tropical Pacific planktonic and benthic foraminiferal test size during the Paleocene-Eocene thermal Maximum. Palaeogeogr Palaeoclimatol Palaeoecol, 237: 456–464
Kemp D B, Coe A L, Cohen A S, Schwark L. 2005. Astronomical pacing of methane release in the Early Jurassic period. Nature, 437: 396–399
Kemp D B, Coe A L, Cohen A S, Weedon G P. 2011. Astronomical forcing and chronology of the early Toarcian (Early Jurassic) oceanic anoxic event in Yorkshire, UK. Paleoceanography, 26: PA002122
Kennett J P, Stott L D. 1991. Abrupt deep-sea warming, palaeoceanographic changes and benthic extinctions at the end of the Palaeocene. Nature, 353: 225–229
Korbar T, Glumac B, Tesovic B C, Cadieux S B. 2012. Response of a carbonate platform to the Cenomanian-Turonian Drowning and OAE 2: A case study from the Adriatic Platform (Dalmatia, Croatia). J Sediment Res, 82: 163–176
Korte C, Hesselbo S P, Ullmann C V, Dietl G, Ruhl M, Schweigert G, Thibault N. 2015. Jurassic climate mode governed by ocean gateway. Nat Commun, 6: 10015
Kraus M J, Riggins S. 2007. Transient drying during the Paleocene-Eocene Thermal Maximum (PETM): Analysis of paleosols in the Bighorn Basin, Wyoming. Palaeogeogr Palaeoclimatol Palaeoecol, 245: 444–461
Kraus M J, Woody D T, Smith J J, Dukic V. 2015. Alluvial response to the Paleocene-Eocene Thermal Maximum climatic event, Polecat Bench, Wyoming (U.S.A.). Palaeogeogr Palaeoclimatol Palaeoecol, 435: 177–192
Krencker F N, Lindström S, Bodin S. 2019. AMajor sea-level drop briefly precedes the Toarcian oceanic anoxic event: Implication for Early Jurassic climate and carbon cycle. Sci Rep, 9: 12518
Krencker F N, Bodin S, Suan G, Heimhofer U, Kabiri L, Immenhauser A. 2015. Toarcian extreme warmth led to tropical cyclone intensification. Earth Planet Sci Lett, 425: 120–130
Leckie R M, Bralower T J, Cashman R. 2002. Oceanic anoxic events and plankton evolution: Biotic response to tectonic forcing during the mid-Cretaceous. Paleoceanography, 17: 13-1–13-29
Li F, Wang X, Xue W, Yan J. 2010. Origin and environmental significance of giant ooids in the Early Triassic: A new kind of anachronistic facies (in Chinese). Acta Sedimentol Sin, 28: 585–595
Li J, Hu X, Garzanti E, BouDagher-Fadel M. 2017. Shallow-water carbonate responses to the Paleocene-Eocene thermal Maximum in the Tethyan Himalaya (southern Tibet): Tectonic and climatic implications. Palaeogeogr Palaeoclimatol Palaeoecol, 466: 153–165
Li J, Hu X, Zhao K, Cai Y, Sun T. 2016. Paleoceanographic evolution and chronostratigraphy of the Aptian Oceanic Anoxic Event 1a (OAE1a) to oceanic red bed 1 (ORB1) in the Gorgo a Cerbara section (central Italy). Cretac Res, 66: 115–128
Li Y X, Montañez I P, Liu Z, Ma L. 2017. Astronomical constraints on global carbon-cycle perturbation during Oceanic Anoxic Event 2 (OAE2). Earth Planet Sci Lett, 462: 35–46
Li Y X, Bralower T J, Montañez I P, Osleger D A, Arthur M A, Bice D M, Herbert T D, Erba E, Premoli Silva I. 2008. Toward an orbital chronology for the early Aptian Oceanic Anoxic Event (OAE1a, ~120 Ma). Earth Planet Sci Lett, 271: 88–100
Ludvigson G A, Joeckel R M, Gonzalez L A, Gulbranson E L, Rasbury E T, Hunt G J, Kirkland J I, Madsen S. 2010. Correlation of Aptian-Albian carbon isotope excursions in continental strata of the Cretaceous foreland basin, Eastern Utah, U.S.A. J Sediment Res, 80: 955–974
MacLeod K G, Martin E E, Blair S W. 2008. Nd isotopic excursion across Cretaceous ocean anoxic event 2 (Cenomanian-Turonian) in the tropical

North Atlantic. Geology, 36: 811–814
McArthur J M, Donovan D T, Thirlwall M F, Fouke B W, Mattey D. 2000. Strontium isotope profile of the early Toarcian (Jurassic) oceanic anoxic event, the duration of ammonite biozones, and belemnite palaeotemperatures. Earth Planet Sci Lett, 179: 269–285
McElwain J C, Wade-Murphy J, Hesselbo S P. 2005. Changes in carbon dioxide during an oceanic anoxic event linked to intrusion into Gondwana coals. Nature, 435: 479–482
McInerney F A, Wing S L. 2011. The Paleocene-Eocene Thermal Maximum: A perturbation of carbon cycle, climate, and biosphere with implications for the future. Annu Rev Earth Planet Sci, 39: 489–516
Menegatti A P, Weissert H, Brown R S, Tyson R V, Farrimond P, Strasser A, Caron M. 1998. High-resolution $\delta^{13}C$ stratigraphy through the Early Aptian "Livello selli" of the Alpine tethys. Paleoceanography, 13: 530–545
Montañez I P, Osleger D A, Banner J L. 2000. Evolution of the Sr and C isotope composition of Cambrian oceans. GSA today, 10: 1–7
Morten S D, Twitchett R J. 2009. Fluctuations in the body size ofMarine invertebrates through the Pliensbachian-Toarcian extinction event. Palaeogeogr Palaeoclimatol Palaeoecol, 284: 29–38
Mülayim O, Yilmaz O I, Sarı B, Taslı K, Wagreich M. 2019. Cenomanian-Turonian drowning of the Arabian Carbonate Platform, the İnişdere section, Adıyaman, SE Turkey. Geol Soc Lond, 498: SP498-2018-130
Murphy A E, Sageman B B, Hollander D J, Lyons T W, Brett C E. 2000. Black shale deposition and faunal overturn in the Devonian Appalachian Basin: Clastic starvation, seasonal water-column mixing, and efficient biolimiting nutrient recycling. Paleoceanography, 15: 280–291
Murphy B H, Farley K A, Zachos J C. 2010. An extraterrestrial ^{3}He-based timescale for the Paleocene-Eocene thermal Maximum (PETM) from Walvis Ridge, IODP Site 1266. Geochim Cosmochim Acta, 74: 5098–5108
Mutterlose J, Bottini C, Schouten S, Sinninghe Damsté J S. 2014. High sea-surface temperatures during the early Aptian Oceanic Anoxic Event 1a in the Boreal Realm. Geology, 42: 439–442
Mutterlose J, Malkoc M, Schouten S, Sinninghe Damsté J S, Forster A. 2010. TEX_{86} and stable $\delta^{18}O$ paleothermometry of early Cretaceous sediments: Implications for belemnite ecology and paleotemperature proxy application. Earth Planet Sci Lett, 298: 286–298
National Research Council (NRC). 2011. Understanding Earth's Deep Past: Lessons for Our Climate Future. Washington D C: The National Academies Press. 208
Naafs B D A, Pancost R D. 2016. Sea-surface temperature evolution across Aptian Oceanic Anoxic Event 1a. Geology, 44: 959–962
O'Brien C L, Robinson S A, Pancost R D, Sinninghe Damsté J S, Schouten S, Lunt D J, Alsenz H, Bornemann A, Bottini C, Brassell S C, Farnsworth A, Forster A, Huberl B T, Inglis G N, Jenkyns H C, Linnert C, Littler, K,Markwick P, McAnena A, Mutterlose J, Naafs, B D A, Püttmann W, Sluijs A, van Helmond N A G M, Vellekoop J, Wagner T, Wrobel N E. 2017. Cretaceous sea-surface temperature evolution: Constraints from TEX_{86} and planktonic foraminiferal oxygen isotopes. Earth-Sci Rev, 172: 224–247
Ogg J G, Ogg G M, Gradstein F M. 2016. A Concise Geologic Time Scale: 2016. Amsterdam: Elsevier. 240
Pälike C, Delaney M L, Zachos J C. 2014. Deep-sea redox across the Paleocene-Eocene thermal Maximum. Geochem Geophys Geosyst, 15: 1038–1053
Pancost R D, Crawford N, Magness S, Turner A, Jenkyns H C, Maxwell J R. 2004. Further evidence for the development of photic-zone euxinic conditions during Mesozoic oceanic anoxic events. J Geol Soc, 161: 353–364
Patruno S, Triantaphyllou M V, Erba E, Dimiza M D, Bottini C, Kaminski M A. 2015. The Barremian and Aptian stepwise development of the 'Oceanic Anoxic Event 1a' (OAE 1a) crisis: Integrated benthic and planktic high-resolution palaeoecology along the Gorgo a Cerbara stratotype section (Umbria-Marche Basin, Italy). Palaeogeogr Palaeoclimatol Palaeoecol, 424: 147–182
Payne J L, Turchyn A V, Paytan A, Depaolo D J, Lehrmann D J, Yu M, Wei J. 2010. Calcium isotope constraints on the end-Permian Mass extinction. Proc Natl Acad Sci USA, 107: 8543–8548
Pearson P N, Nicholas C J. 2014. Layering in the Paleocene/Eocene boundary of the Millville core is drilling disturbance. Proc Natl Acad Sci USA, 111: E1064–E1065
Penman D E, Hönisch B, Zeebe R E, Thomas E, Zachos J C. 2014. Rapid and sustained surface ocean acidification during the Paleocene-Eocene Thermal Maximum. Paleoceanography, 29: 357–369
Percival L M E, Jenkyns H C, Mather T A, Dickson A J, Batenburg S J, Ruhl M, Hesselbo S P, Barclay R, Jarvis I, Robinson S A, Woelders L. 2018. Does large igneous province volcanism always perturb the mercury cycle? Comparing the records of Oceanic Anoxic Event 2 and the end-Cretaceous to other Mesozoic events. Am J Sci, 318: 799–860
Pogge von Strandmann P A E, Jenkyns H C, Woodfine R G. 2013. Lithium isotope evidence for enhanced weathering during Oceanic Anoxic Event 2. Nat Geosci, 6: 668–672
Pujalte V, Schmitz B, Baceta J I. 2014. Sea-level changes across the Paleocene-Eocene interval in the Spanish Pyrenees, and their possible relationship with North AtlanticMagmatism. Palaeogeogr Palaeoclimatol Palaeoecol, 393: 45–60
Racki G, Rakociński M, Marynowski L, Wignall P B. 2018. Mercury enrichments and the Frasnian-Famennian biotic crisis: A volcanic trigger proved? Geology, 46: 543–546
Röhl U, Norris R, Ogg J G. 2003. Cyclostratigraphy of upper Paleocene and lower Eocene sediments at Blake Nose Site 1051 (western North Atlantic). Geol Soc Am Spec Pap, 369: 567–588
Röhl U, Westerhold T, Bralower T J, Zachos J C. 2007. On the duration of the Paleocene-Eocene thermal Maximum (PETM). Geochem Geophys Geosyst, 8: Q12002
Robinson S A, Heimhofer U, Hesselbo S P, Petrizzo M R. 2017. Mesozoic climates and oceans: A tribute to Hugh Jenkyns and Helmut Weissert. Sedimentology, 64: 1–15
Rong J, Huang B. 2014. Study of Mass Extinction over the past thirty years: A synopsis (in Chinese). Sci Sin Terr, 44: 377–404
Ruebsam W, Münzberger P, Schwark L. 2014. Chronology of the early Toarcian environmental crisis in the Lorraine Sub-Basin (NE Paris Basin). Earth Planet Sci Lett, 404: 273–282
Sabatino N, Vlahović I, Jenkyns H C, Scopelliti G, Neri R, Prtoljan B, Velić I. 2013. Carbon-isotope record and palaeoenvironmental changes during the early Toarcian oceanic anoxic event in shallow-marine carbonates of the Adriatic Carbonate Platform in Croatia. Geol Mag, 150: 1085–1102
Sageman B B, Meyers S R, Arthur M A. 2006. Orbital time scale and new C-isotope record for Cenomanian-Turonian boundary stratotype. Geology, 34: 125–128
Scheibner C, Speijer R P. 2008. Decline of coral reefs during late Paleocene to early Eocene global warming. EEarth, 3: 19–26
Scheibner C, Speijer R P, Marzouk A M. 2005. Turnover of larger foraminifera during the Paleocene-Eocene Thermal Maximum and paleoclimatic control on the evolution of platform ecosystems. Geology, 33: 493–496
Schmitz B, Pujalte V. 2003. Sea-level, humidity, and land-erosion records across the initial Eocene thermal Maximum from a continental-marine transect in northern Spain. Geology, 31: 689–692
Schmitz B, Pujalte V. 2007. Abrupt increase in seasonal extreme precipitation at the Paleocene-Eocene boundary. Geology, 35: 215–218
Sepkoski Jr J J. 1996. Patterns of Phanerozoic extinction: A perspective from global data bases, Global events and event stratigraphy in the Phanerozoic. In: Walliser O, H, ed. Global Events and Event Stratigraphy in the Phanerozoic. Berlin: Springer-Verlag. 35–51
Shen S, Crowley J L, Wang Y, Bowring S A, Erwin D H, Sadler P M, Cao C, Rothman D H, Henderson C M, Ramezani J, Zhang H, Shen Y, Wang X, Wang W, Mu L, Li W, Tang Y, Liu X, Liu L, Zeng Y, Jiang Y, Jin Y. 2011. Calibrating the end-Permian Mass extinction. Science, 334: 1367–1372
Shen S Z, Ramezani J, Chen J, Cao C Q, Erwin D H, Zhang H, Xiang L, Schoepfer S D, Henderson C M, Zheng Q F, Bowring S A, Wang Y, Li

X H, Wang X D, Yuan D X, Zhang Y C, Mu L, Wang J, Wu Y S. 2019. A sudden end-Permian Mass extinction in South China. GSA Bull, 131: 205–223
Shen S, Zhang H. 2017. What caused the five mass extinctions (in Chinese)? Chin Sci Bull, 62: 1119–1135
Simms M J, Ruffell A H. 1989. Synchroneity of climatic change and extinctions in the Late Triassic. Geology, 17: 265–268
Sinninghe Damsté J S, van Bentum E C, Reichart G J, Pross J, Schouten S. 2010. A CO_2 decrease-driven cooling and increased latitudinal temperature gradient during the mid-Cretaceous Oceanic Anoxic Event 2. Earth Planet Sci Lett, 293: 97–103
Skelton P W, Gili E. 2012. Rudists and carbonate platforms in the Aptian: A case study on biotic interactions with ocean chemistry and climate. Sedimentology, 59: 81–117
Sluijs A, Bijl P K, Schouten S, Röhl U, Reichart G J, Brinkhuis H. 2011. Southern ocean warming, sea level and hydrological change during the Paleocene-Eocene thermal Maximum. Clim Past, 7: 47–61
Sluijs A, Brinkhuis H. 2009. A dynamic climate and ecosystem state during the Paleocene-Eocene Thermal Maximum: Inferences from dinoflagellate cyst assemblages on the New Jersey Shelf. Biogeosciences, 6: 1755–1781
Sluijs A, Röhl U, Schouten S, Brumsack H J, Sangiorgi F, Sinninghe Damsté J S, Brinkhuis H. 2008. Arctic late Paleocene-early Eocene paleoenvironments with special emphasis on the Paleocene-Eocene thermal Maximum (Lomonosov Ridge, Integrated Ocean Drilling Program Expedition 302). Paleoceanography, 23: PA1S11
Sluijs A, Schouten S, Pagani M, Woltering M, Brinkhuis H, Sinninghe Damsté J S, Dickens G R, Huber M, Reichart G J, Stein R, Matthiessen J, Lourens L J, Pedentchouk N, Backman J, Moran K. 2006. Subtropical Arctic Ocean temperatures during the Palaeocene/Eocene thermal Maximum. Nature, 441: 610–613
Sluijs A, van Roij L, Harrington G J, Schouten S, Sessa J A, LeVay L J, Reichart G J, Slomp C P. 2014. Warming, euxinia and sea level rise during the Paleocene-Eocene Thermal Maximum on the Gulf Coastal Plain: Implications for ocean oxygenation and nutrient cycling. Clim Past, 10: 1421–1439
Socorro J, Maurrasse F J M R, Sanchez-Hernandez Y. 2017. Characterization of the negative carbon isotope shift in segment C_2, its global implications as a harbinger of OAE1a. Sci China Earth Sci, 60: 30–43
Song H, Tong J. 2016. Mass extinction and survival during the Permian-Triassic crissis (in Chinese). Earth Sci, 41: 901–918
Song H, Wignall P B, Tong J, Yin H. 2013. Two pulses of extinction during the Permian-Triassic crisis. Nat Geosci, 6: 52–56
Speijer R P, Wagner T. 2002. Sea-level changes and black shales associated with the late Paleocene thermal Maximum (LPTM): Organic geochemical and micropaleontologic evidence from the southern TethyanMargin (Egypt-Israel). Geol Soc Amer Spec Pap, 356: 522–550
Stanley G D. 1989. An Upper Triassic reefal limestone, Southern Vancouver Island, B.C. In: Geldsetzer H H J, James N P, Tebbutt G E, eds. Reef: Canada and Adjacent Areas. Canadian Society of Petroleum Geologists. Memoirs, 13: 766–775
Stein M, Westermann S, Adatte T, Matera V, Fleitmann D, Spangenberg J E, Föllmi K B. 2012. Late Barremian-Early Aptian palaeoenvironmental change: The Cassis-La Bédoule section, southeast France. Cretac Res, 37: 209–222
Suan G, Mattioli E, Pittet B, Lécuyer C, Suchéras-Marx B, Duarte L V, Philippe M, Reggiani L, Martineau F. 2010. Secular environmental precursors to Early Toarcian (Jurassic) extreme climate changes. Earth Planet Sci Lett, 290: 448–458
Suan G, Mattioli E, Pittet B, Mailliot S, Lécuyer C. 2008a. Evidence for-Major environmental perturbation prior to and during the Toarcian (Early Jurassic) oceanic anoxic event from the Lusitanian Basin, Portugal. Paleoceanography, 23: PA001202
Suan G, Pittet B, Bour I, Mattioli E, Duarte L, Mailliot S. 2008b. Duration of the Early Toarcian carbon isotope excursion deduced from spectral analysis: Consequence for its possible causes. Earth Planet Sci Lett, 267: 666–679
Suarez M B, Ludvigson G A, González L A, You H L. 2017. Continental paleotemperatures from an early Cretaceous dolomitic lake, Gansu province, China. J Sediment Res, 87: 486–499
Sun Y, Joachimski M M, Wignall P B, Yan C, Chen Y, Jiang H, Wang L, Lai X. 2012. Lethally hot temperatures during the early Triassic Greenhouse. Science, 338: 366–370
Sun Y D, Richoz S, Krystyn L, Zhang Z T, Joachimski M M. 2019. Perturbations in the carbon cycle during the Carnian Humid Episode: Carbonate carbon isotope records from southwestern China and northern Oman. J Geol Soc, 176: 167–177
Takeda K, Kaiho K. 2007. Faunal turnovers in central Pacific benthic foraminifera during the Paleocene-Eocene thermal Maximum. Palaeogeogr Palaeoclimatol Palaeoecol, 251: 175–197
Thomas D J, Zachos J C, Bralower T J, Thomas E, Bohaty S. 2002. Warming the fuel for the fire: Evidence for the thermal dissociation of methane hydrate during the Paleocene-Eocene thermal Maximum. Geology, 30: 1067–1070
Trecalli A, Spangenberg J, Adatte T, Föllmi K B, Parente M. 2012. Carbonate platform evidence of ocean acidification at the onset of the early Toarcian oceanic anoxic event. Earth Planet Sci Lett, 357: 214–225
Turner S K. 2018. Constraints on the onset duration of the Paleocene-Eocene Thermal Maximum. Phil Trans R Soc A, 376: 20170082
van Bentum E C, Hetzel A, Brumsack H J, Forster A, Reichart G J, Sinninghe Damsté J S. 2009. Reconstruction of water column anoxia in the equatorial Atlantic during the Cenomanian-Turonian oceanic anoxic event using biomarker and trace metal proxies. Palaeogeogr Palaeoclimatol Palaeoecol, 280: 489–498
van Helmond N A G M, Ruvalcaba Baroni I, Sluijs A, Sinninghe Damsté J S, Slomp C P. 2014. Spatial extent and degree of oxygen depletion in the deep proto-North Atlantic basin during Oceanic Anoxic Event 2. Geochem Geophys Geosyst, 15: 4254–4266
Wang C, Wang T, Chen X, Gao Y, Zhang L. 2017. Paleoclimate implications for future climate change (in Chinese). Earth Sci Front, 24: 1–17
Ward P D, Botha J, Buick R, De Kock M O, Erwin D H, Garrison G H, Kirschvink J L, Smith R. 2005. Abrupt and gradual extinction among late Permian land vertebrates in the Karoo Basin, South Africa. Science, 307: 709–714
Ward P D, Montgomery D R, Smith R. 2000. Altered river morphology in South Africa related to the Permian-Triassic extinction. Science, 289: 1740–1743
Waters C N, Zalasiewicz J, Summerhayes C, Barnosky A D, Poirier C, Gałuszka A, Cearreta A, Edgeworth M, Ellis E C, Ellis M, Jeandel C, Leinfelder R, McNeill J R, Richter D B, Steffen W, Syvitski J, Vidas D, Wagreich M, Williams M, Zhisheng A, Grinevald J, Odada E, Oreskes N, Wolfe A P. 2016. The Anthropocene is functionally and stratigraphically distinct from the Holocene. Science, 351: aad2622
Westerhold T, Röhl U, Donner B, Zachos J C. 2018. Global extent of early Eocene hyperthermal events: A new Pacific benthic foraminiferal isotope record from Shatsky Rise (ODP Site 1209). Paleoceanogr Paleoclimatol, 33: 626–642
Westermann S, Stein M, Matera V, Fiet N, Fleitmann D, Adatte T, Föllmi K B. 2013. Rapid changes in the redox conditions of the western Tethys Ocean during the early Aptian oceanic anoxic event. Geochim Cosmochim Acta, 121: 467–486
Wignall P B. 2001. Large igneous provinces and Mass extinctions. Earth-Sci Rev, 53: 1–33
Wilson E O, MacArthur R H. 1967. The Theory of Island Biogeography. Princeton N J: Princeton University Press
Wing S L, Harrington G J, Smith F A, Bloch J I, Boyer D M, Freeman K H. 2005. Transient floral change and rapid global warming at the Paleocene-Eocene boundary. Science, 310: 993–996
Winguth A M E, Thomas E, Winguth C. 2012. Global decline in ocean ventilation, oxygenation, and productivity during the Paleocene-Eocene Thermal Maximum: Implications for the benthic extinction. Geology, 40: 263–266
Wright J D, Schaller M F. 2013. Evidence for a rapid release of carbon at

the Paleocene-Eocene thermal Maximum. Proc Natl Acad Sci USA, 110: 15908–15913
Xu B, Gu Z, Wang C, Hao Q, Han J, Liu Q, Wang L, Lu Y. 2012. Carbon isotopic evidence for the associations of decreasing atmospheric CO_2 level with the Frasnian-Famennian Mass extinction. J Geophys Res, 170: 1–12
Yin H, Jiang H, Xia W, Feng Q, Zhang N, Shen J. 2014. The end-Permian regression in South China and its implication on Mass extinction. Earth-Sci Rev, 137: 19–33
Yu J, Broutin J, Chen Z Q, Shi X, Li H, Chu D, Huang Q. 2015. Vegetation changeover across the Permian-Triassic boundary in southwest China. Earth-Sci Rev, 149: 203–224
Zachos J, Pagani M, Sloan L, Thomas E, Billups K. 2001. Trends, rhythms, and aberrations in global climate 65 Ma to present. Science, 292: 686–693
Zachos J C, Röhl U, Schellenberg S A, Sluijs A, Hodell D A, Kelly D C, Thomas E, Nicolo M, Raffi I, Lourens L J, McCarren H, Kroon D. 2005. Rapid acidification of the ocean during the Paleocene-Eocene Thermal Maximum. Science, 308: 1611–1615
Zachos J C, Schouten S, Bohaty S, Quattlebaum T, Sluijs A, Brinkhuis H, Gibbs S J, Bralower T J. 2006. Extreme warming of mid-latitude coastal ocean during the Paleocene-Eocene Thermal Maximum: Inferences from TEX_{86} and isotope data. Geology, 34: 737–740
Zachos J C, Wara M W, Bohaty S, Delaney M L, Petrizzo M R, Brill A, Bralower T J, Premoli-Silva I. 2003. A transient rise in tropical sea surface temperature during the Paleocene-Eocene thermal Maximum. Science, 302: 1551–1554
Zeebe R E, Dickens G R, Ridgwell A, Sluijs A, Thomas E. 2014. Onset of carbon isotope excursion at the Paleocene-Eocene thermal Maximum took millennia, not 13 years. Proc Natl Acad Sci USA, 111: E1062–E1063
Zeebe R E, Zachos J C, Dickens G R. 2009. Carbon dioxide forcing alone insufficient to explain Palaeocene–Eocene Thermal Maximum warming. Nat Geosci, 2: 576–580
Zhao X M, Tong J N, Yao H Z, Zhang K X, Chen Z Q. 2008. Anachronistic facies in the Lower Triassic of South China and their implications to the ecosystems during the recovery time. Sci China Ser D-Earth Sci, 51: 1646–1657
Zheng X Y, Jenkyns H C, Gale A S, Ward D J, Henderson G M. 2013. Changing ocean circulation and hydrothermal inputs during Ocean Anoxic Event 2 (Cenomanian-Turonian): Evidence from Nd-isotopes in the European shelf sea. Earth Planet Sci Lett, 375: 338–348
Zhu Z, Liu Y, Kuang H, Benton M J, Newell A J, Xu H, An W, Ji S, Xu S, Peng N, Zhai Q. 2019. Altered fluvial patterns in North China indicate rapid climate change linked to the Permian-Triassic Mass extinction. Sci Rep, 9: 16818
Zhuravlev A Y, Wood R A. 1996. Anoxia as the cause of the mid-Early Cambrian (Botomian) extinction event. Geology, 24: 311–314

(Responsible editor: Jianfang HU)